THE PRODUCTION AND OPTICAL INVESTIGATION OF ION-DOPED SOL-GEL-DERIVED SILICA

BY

PAULINE MARRON B.Sc.

A THESIS PRESENTED TO

DUBLIN CITY UNIVERSITY

FOR THE DEGREE OF

MASTER OF SCIENCE

AUGUST 1993

SUPERVISOR : Dr COLETTE Mc DONAGH

DEDICATION

This thesis is dedicated to my mother, to the memory of my father, and to Teri.

ACKNOWLEDGEMENTS.

I wish to thank so many people for their help through the course of my MSc study. Monaghan county council for their funding for the past six years. My family, especially Mary O'Sullivan who listened to my tales of woe and physics. I wish to thank Colette McDonagh whose friendship and encouragement I will always value. Thanks also to John, Tang and Brendan in Trinity for their help in sample production and analysis. And of course the lads an lasses that make up the physics postgraduate body in D.C.U. Especially Paul Kiernan, Brian Hurley, Charles Markham, Ger Ennis, Ger O'Keeffe and Kevin Devlin for their help during the course of the work.

ABSTRACT

This thesis describes the synthesis of sol-gel glass materials under different experimental conditions and the result of doping these materials with optical probes. The probes used were Eu^{3+}, UO_2^{2+} and Cr^{3+}. Changes in optical parameters such as fluorescence, absorption and decay times were used to determine the structure of the material. Eu^{3+} was easily incorporated into the silica structure. The fluorescence spectra and decay times measured were used to evaluate structural changes of the ion matrix. The use of UO_2^{2+} as a probe is investigated in this study. UO_2^{2+} was used as an optical pump for Eu^{3+} when codoped in silica. and energy transfer effects were used to investigate the porosity.

DECLARATION This thesis is based on my own work.

CONTENTS

CHAPTER 1 The structure of glass	PAGE
1.1 Introduction	4
1.2 The nature of glass	4
1.3 Conventional glass production	4
1.4 Products of the sol-gel process	6
1.5 Summary	7
CHAPTER 2 The sol-gel process.	
2.1 Introduction	8
2.2 Sol-gel processing steps	8
2.3 Hydrolysis and condensation	11
2.4 Gelation	15
2.5 Aging	15
2.6 Drying	16
2.7 Stabilisation	16
2.8 Densification	17
2.9 Summary	17
CHAPTER 3 Fluorescence spectroscopy	
3.1 Introduction	18
3.2 Absorption and fluorescence transitions	18
3.3 The nature of fluorescent materials	19
3.4 Electron energy levels	19
3.5 Electronic spectra	20
3.6 Radiative and non radiative transitions	23

3.7 Optically active ions 23
3.8 Europium as a fluorescence probe 24
3.9 Chromium as a fluorescence probe 25
3.10 Uranyl ion as a fluorescence probe 29
3.11 Summary 31

CHAPTER 4 Sol-gel glass production and experimental techniques

4.1 Introduction 32
4.2 Synthesis of silica gels 32
4.3 Optimum ion concentration 33
4.4 Fluorescence data aquisition 33
4.5 Lifetime measurements 34
4.6 Lifetime calculation 36
4.7 Summary 37

CHAPTER 5 Europium and chromium doped samples

5.1 Introduction 38
5.2 Eu^{3+}Samples produced for analysis 38
5.3 Fluorescence studies as a function of drying temperature 39
5.4 Fluorescence studies as a function of pH 46
5.5 Fluorescence studies as a function of r 48
5.6 Samples soaked in D_2O 48
5.7 Chromium as a Sol-Gel Probe 50
5.8 Conclusion 53

CHAPTER 6 Uranyl doped sol-gel materials

6.1 Introduction 55
6.2 Optimum concentration determination 55
6.3 Samples produced for analysis 55

6.4 Spectral variations as a function of temperature 56
6.5 Spectral variation with pH 62
6.6 Spectral variation as a function of r 63
6.7 Samples quenched in D_2o 63
6.8 Comparison of Eu^{3+} and UO_2^{2+} as structural probes 64
6.9 Summary 65

CHAPTER 7 Europium/uranyl codoped materials, and energy transfer effect

7.1 Introduction 66
7.2 Energy transfer in solids 66
7.3 Samples prepared for energy transfer studies 67
7.4 Fluorescence and decay times of co-doped materials 68
7.5 Samples soaked in $Eu(NO_3)_3$ (post-doped) 74
7.6 Summary 79

CHAPTER 8 Conclusions and proposals for future work 80

REFERENCES 81

APPENDIX 1 Program listing "Aver2" 83
APPENDIX 2 Program listing "Lifet" 87
APPENDIX 3 Program listing "Compstw" 90

CHAPTER 1

THE STRUCTURE OF GLASS

1.1 Introduction

The nature of the glassy state and methods of glass production will be discussed in this chapter. A comparison will be made between the available methods of glass production and a synopsis of sol-gel glass production provided.

1.2 The Nature of Glass

The term glass is commonly used to mean the fusion product of inorganic materials which have cooled to a rigid condition without crystallising. Glass formation is not an atomic or molecular property but rather one of a state of aggregation.

Glasses are characterised by certain well defined properties which are different from those of liquids and crystalline solids. X-ray and electron diffraction studies show that glasses lack the long range periodic order of crystals in the distribution of their constituent atoms. They resemble liquids in their atomic distribution as illustrated in fig 1.1. in which the radial distribution function of a hypothetical material in the glassy state is compared with that of the gas, liquid and crystalline state of the same composition.[1]

1.3 Conventional Glass Production

Of all the elements in the periodic table only a few in group V and VI can form glass on their own; P, O, S, Se, Te. Some oxides also form glasses; B_2O_3, SiO_2, GeO_2, and P_2O_5 readily form glasses on their own and are commonly known as 'glass formers' for they provide the backbone in mixed oxide glasses[1].

Traditional methods of glass making involve mixing sand (SiO_2), soda (Na_2CO_3) and lime ($CaCO_3$) which is then cured at a high temperature and cooled rapidly. In recent years there have been many advances in the techniques used in glass making mainly in chemical vapour deposition and sol-gel processing [2]. The sol-gel process has advantages over conventional glass production methods, namely higher product purity,

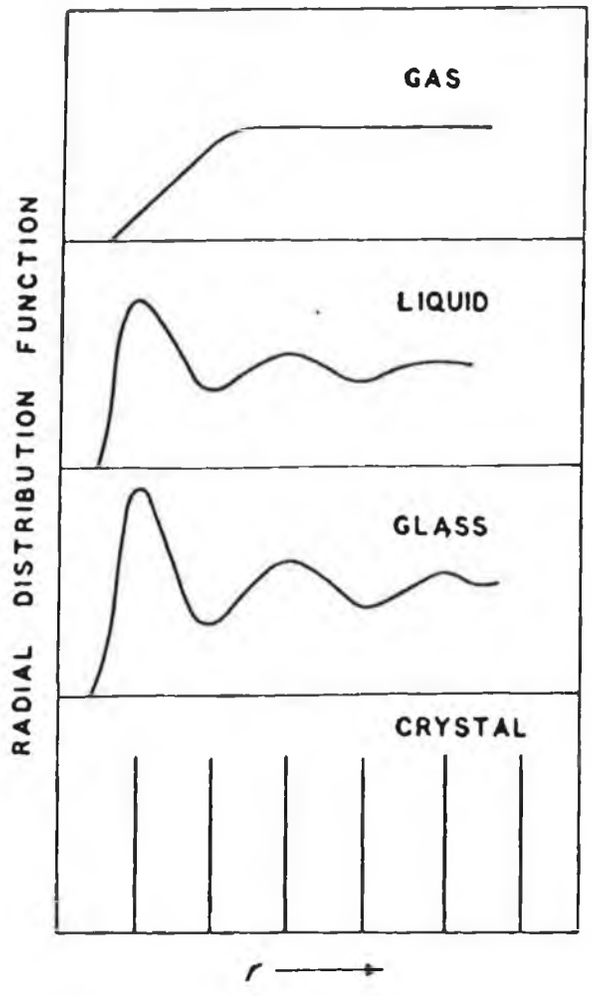

Figure 1.1 Atomic Distribution Comparisons for various Materials

more control over pore size and a wider variety of final products. Currently, however, conventional glass ages better. Normal 'melting' is generally more cost efficient and the conventional raw materials are inexpensive as is the equipment required such as crucible and furnace. Disadvantages of the conventional process include the following:

-the refractory nature of the material which implies very high melting temperatures (e.g. glasses rich in Al_2O_3, SiO_2, TiO_2)

- low reactivity of raw materials (CaO, SiO_2)

- volatility or instability of constituents of the glass or of raw materials (e.g. halides, chalcogenides, boron compounds)

-difficulty in melting, segregation, and in homogeneity[2].

Sol-gel methods rely on the ease with which homogenous solutions or suspensions of fine particles can be produced at low temperatures, turned into gels and eventually sintered and consolidated at viscosities much higher than normal glass melting would have required, and hence at lower temperatures. [2]

1.4 Products of the Sol-Gel Process

The most common sol-gel process for making glass utilises monomeric alkoxide precursors. In solution, the alkoxides are hydrolysed and condensed to form polymeric species composed of M-O-M bonds, where M is a metal, for example silicon. At the functional group level, three reactions are generally used to describe the sol-gel process as shown below for silicon:

Hydrolysis $\equiv SiOR + H_2O \rightleftharpoons \equiv SiOH + ROH$ **(1.1)**

Condensation $\equiv SiOH + HOSi\equiv \rightleftharpoons \equiv SiOSi + H_2O$ **(1.2)**

Condensation $\equiv SiOR + HOSi\equiv \rightleftharpoons \equiv SiOSi + ROH$ **(1.3)**

where R is an alkyl group, for example CH_3 or C_2H_5. It is evident from equations 1.1 to 1.3 that the structure of sol-gel glasses evolves sequentially as the product of successive hydrolysis and condensation reactions[3].

Three methods are used to produce monoliths by the sol-gel process:

1. Gelation of a solution of colloidal powders.
2. Hydrolysis and condensation of alkoxide or nitrate precursors followed by hypercritical drying of gels.
3. Hydrolysis and condensation of alkoxide precursors followed by aging and drying under ambient atmospheres.

Sols are defined as dispersions of colloidal particles in liquid. Colloids are solid particles with diameters of 1-100nm. A gel is an interconnected, rigid network with pores of submicron dimensions and polymeric chains whose average length is greater than a micron. A silica gel may be formed from a solution of discrete colloidal particles (method 1) or by the formation of an interconnected 3-D network by simultaneous hydrolysis and condensation of an organometallic precursor (methods 2 and 3).

When the pore liquid is removed from the interconnected solid gel network under hypercritical conditions (critical point drying, method 2) the network does not collapse and a low density aerogel is produced. Aerogels have pore volumes as large as 98% and densities as low as $80kgm^{-3}$. When pore liquid is removed at near ambient pressure by thermal evaporation and shrinkage occurs, the product is termed a xerogel. A gel is termed dry when the physically adsorbed water evaporates. This occurs between 100°C and 180°C. The dried gel still contains a large concentration of chemisorbed hydroxyls on the surface of the pores. Thermal treatment in the range 500-800°C desorbs the hydroxyls[4].

1.5 Summary

This chapter presented some methods of glass production currently being used. It also provided some insight into the nature of glassy structures. Sol-gel derived materials have many advantages over conventional glasses as discussed above. However they are still new and many questions remain unanswered regarding their detailed structure and evolution as a function of processing parameters. The aim of this work is to investigate the use of optical probes as a means of structural determination of sol-gel materials.

CHAPTER 2

THE SOL-GEL PROCESS

2.1 Introduction

This chapter summarises the steps involved in the sol gel process. The aim is to outline the steps involved and to explain why there is a variety of possible final products from the process.

2.2 Sol-Gel Processing Steps

The processing steps involved in making sol-gel-derived silica materials by methods 1 to 3 as stated in section 1.3 are compared below. A schematic illustration of these steps is given in figure 2.1. At step 4 in the process the product of method 1, dried colloidal gel-silica, is produced. Relatively speaking the production of the alkoxide precursor takes twice as long and involves the further steps of ageing and drying. It can be noted from figure 2.1 that production method 3 involves all 7 processing steps,producing a dehydrated and densified final product.

Step 1 : Mixing : In method 1 a sol is formed by mechanical mixing of colloidal particles in water at a pH that prevents precipitation. In methods 2 and 3 a liquid alkoxide precursor such as $Si(OR)_4$ where R is CH_3, C_2H_5 or C_3H_7, is hydrolysed by mixing with water. One such precursor is tetraethylorthosilicate (TEOS) or $Si(OC_2H_5)_4$. The reaction is as follows:

$$TEOS + 4(H_2O) \rightarrow Si(OH)_4 + 4(C_2H_5OH) \qquad (2.1)$$

The hydrated silica tetrahedra interact in a condensation reaction forming silica chains with the elimination of water. Linkage of additional Si-OH tetrahedra occurs as a condensation reaction (figure 2.2) and eventually results in a SiO_2 network. The water and alcohol expelled from the reaction remain in the pores of the network. The hydrolysis and condensation reactions are initiated at numerous sites within the TEOS + H_2O solution as mixing occurs. When sufficient interconnected Si-O-Si bonds are

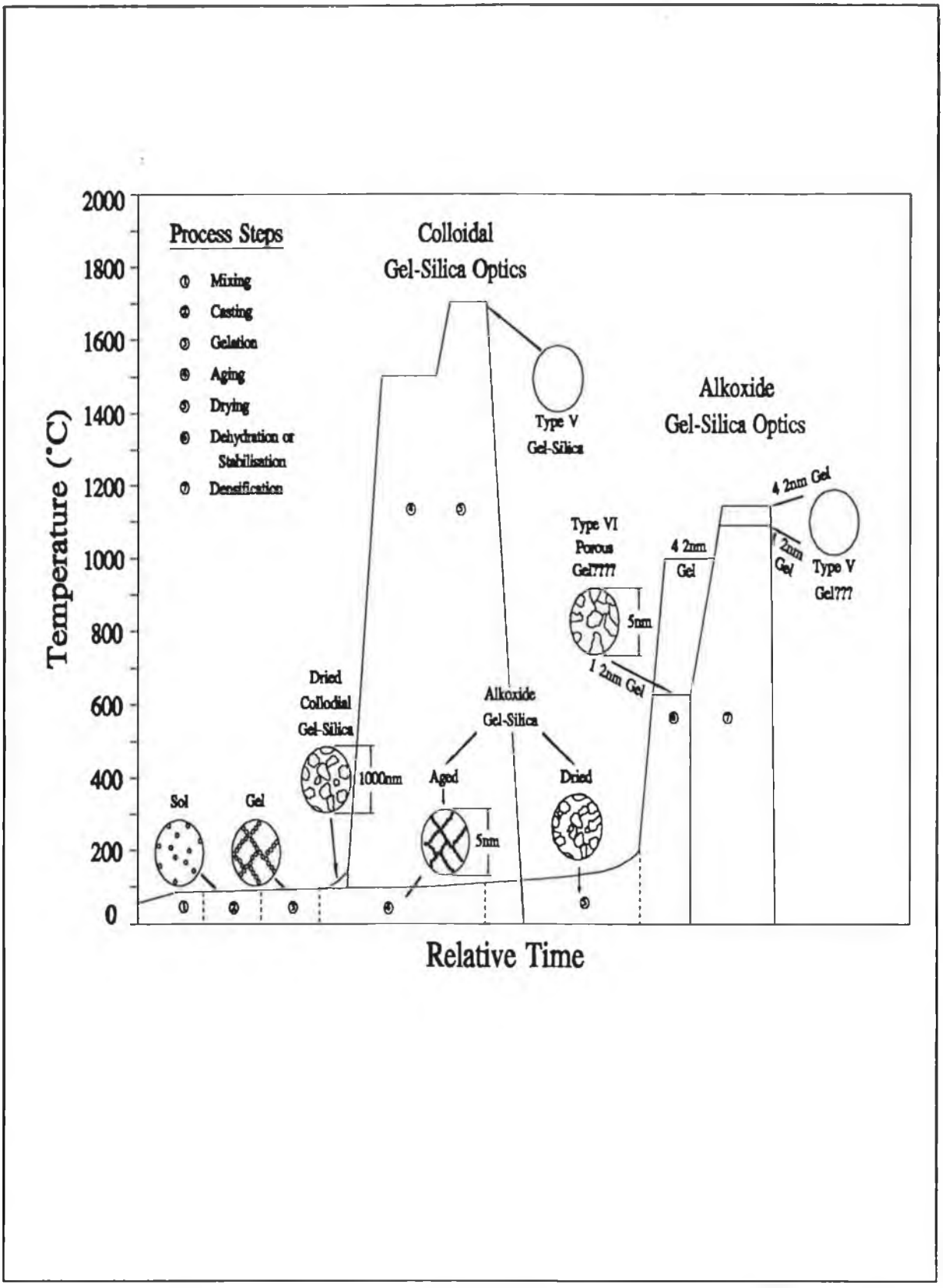

FIGURE 2.1 Structural Development of Sol Gel derived Silica

formed in a region they respond cooperatively as colloidal particles or a sol. The size of the sol particles and cross linkages within the particles depend upon the pH and r ratio, where r is the molar ratio of water to TEOS.

Step 2 : Casting : The sol is cast into a mould. The mould is selected to avoid adhesion of the gel.

Step 3 : Gelation : As time progresses the colloidal particles and condensed silica species link together to become a three-dimensional network. The physical characteristics of the gel network depend greatly on the size of the particles and the extent of the cross-linking prior to gelation.

Step 4 : Aging : Aging of a gel involves maintaining the gel for a period of time, hours to days, completely immersed in a liquid. During aging condensation continues along with localised solution and reprecipitation of the gel network, which increases the thickness of the interparticle necks and decreases the porosity. The strength of the gel thereby increases with aging. An aged gel must develop sufficient strength to resist cracking during drying[1].

Step 5 : Drying : During drying the liquid is removed from the interconnected pore network. Small pores of less than 20nm can develop large capillary stresses during drying. These stresses will cause the gel to crack catastrophically unless the drying process is controlled to decrease the liquid surface energy. This can be achieved by addition of surfactants or elimination of very small pores (method 1), by hypercritical evaporation which avoids the solid-liquid interface (method 2), or by obtaining monodisperse pore sizes by controlling the rates of hydrolysis and condensation (method 3).

Step 6 : Dehydration or chemical stabilization : The removal of surface silanol (Si-OH) groups and physisorbed water from the pore network results in a chemically stable ultra-porous solid. The physisorbed water can be eliminated and silanol groups condensed above 100°C as discussed in section 2.7.

Step 7 : Densification : Heating the porous gel at high temperatures causes densification to occur. The pores are eliminated by collapse of the network and the density ultimately becomes equivalent to fused quartz or fused silica. The densification temperature depends considerably on the dimensions of the pore network, the connectivity of the pore network and surface area as indicated in fig. 2.1. Details of these processing steps follow. The emphasis is on sol gel derived silica monoliths made by the alkoxide process (method 3) at ambient pressure.

2.3 Hydrolysis and Condensation

As shown in fig 2.1, the structure of a gel is established at the time of gelation. Subsequent processes such as aging, drying, stabilisation and densification all depend upon the gel structure. Since the relative rates of hydrolysis and condensation determine the structure of the gel, it is essential to understand the kinetics of the hydrolysis and condensation reactions and the ratio of their rate constants K_H/K_C. The reactions involved in hydrolysis and condensation are shown in Fig. 2.2. Many factors influence the kinetics. Figure 2.3 displays the relationship between pH and hydrolysis and condensation rates. It can be observed that the rate of condensation is at a minimum between pH 1 and 2 while the time taken for complete hydrolysis decreases rapidly above pH 4. Hydrolysis is also enhanced by increasing water concentration. It is obvious that the systems are considerably more complex than represented by the processes in figure 2.2. Many species are present in the solution and furthermore, hydrolysis and condensation occur simultaneously. The variables of major importance are temperature, nature and concentration of electrolyte (acid,base), nature of the solvent, and type of alkoxide precursor. Pressure influences the gelation process, but pressure is usually not a processing variable [1]. It has been found that K_H, the hydrolysis rate constant, increases linearly with the concentration of H^+ or H_3O^+ in acidic media and with concentration of OH^- in basic media[2]. The nature of the solvent (methanol, ethanol) has a "secondary" effect on K_H, so also has the temperature of the reaction, e.g. there is a 10 fold increase in K_H when the temperature increases from 20°C to 45.5°C)[3]. NMR experiments [4] shows that K_H varies in the different solvents as follows: acetonitrile> methanol> dimethyl formamide> dioxane> formamide with K_H (acetontrile) being 20 times larger than K_H (formamide)[1].

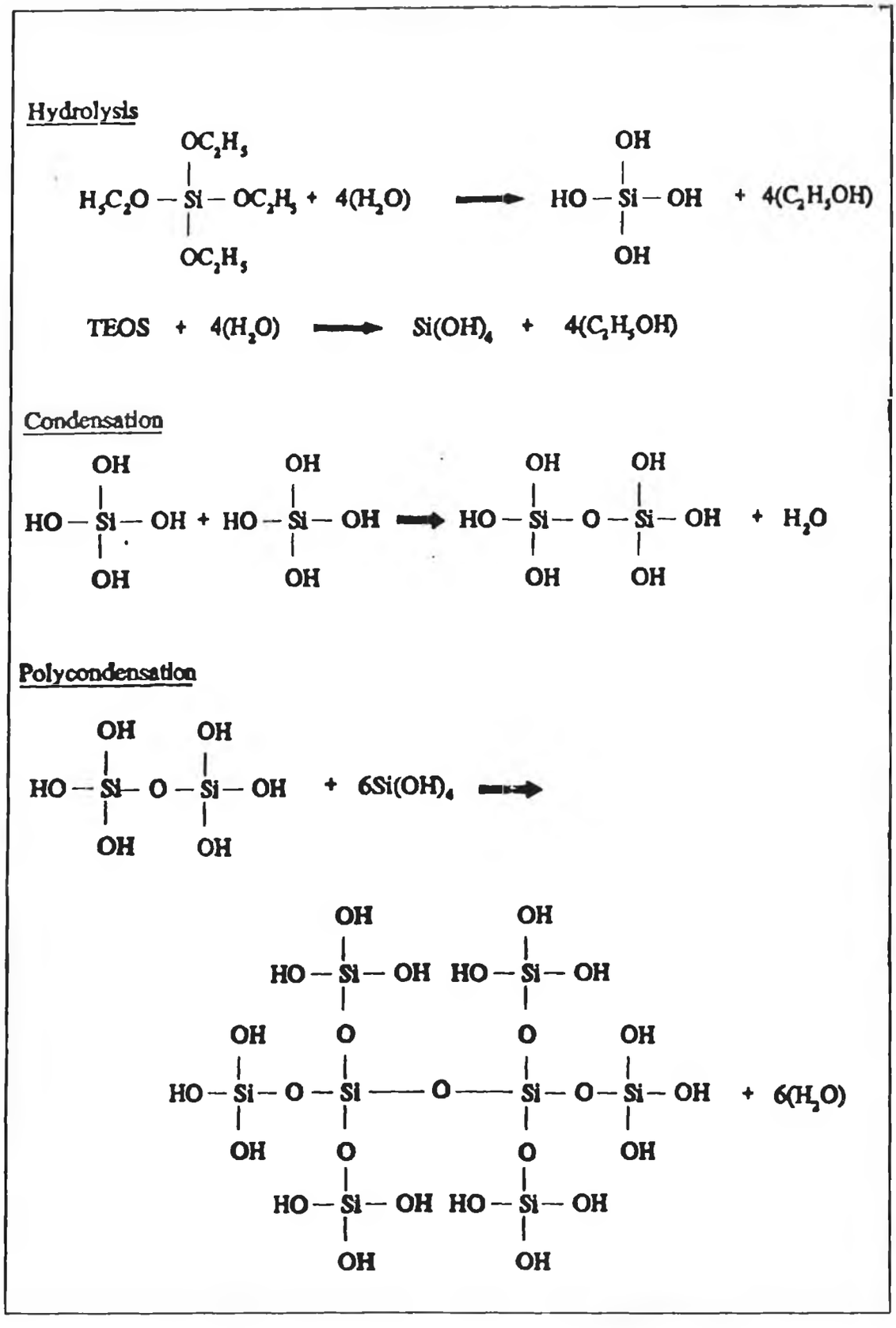

FIGURE 2.2 Hydrolysis and Condensation in the Sol-Gel Process

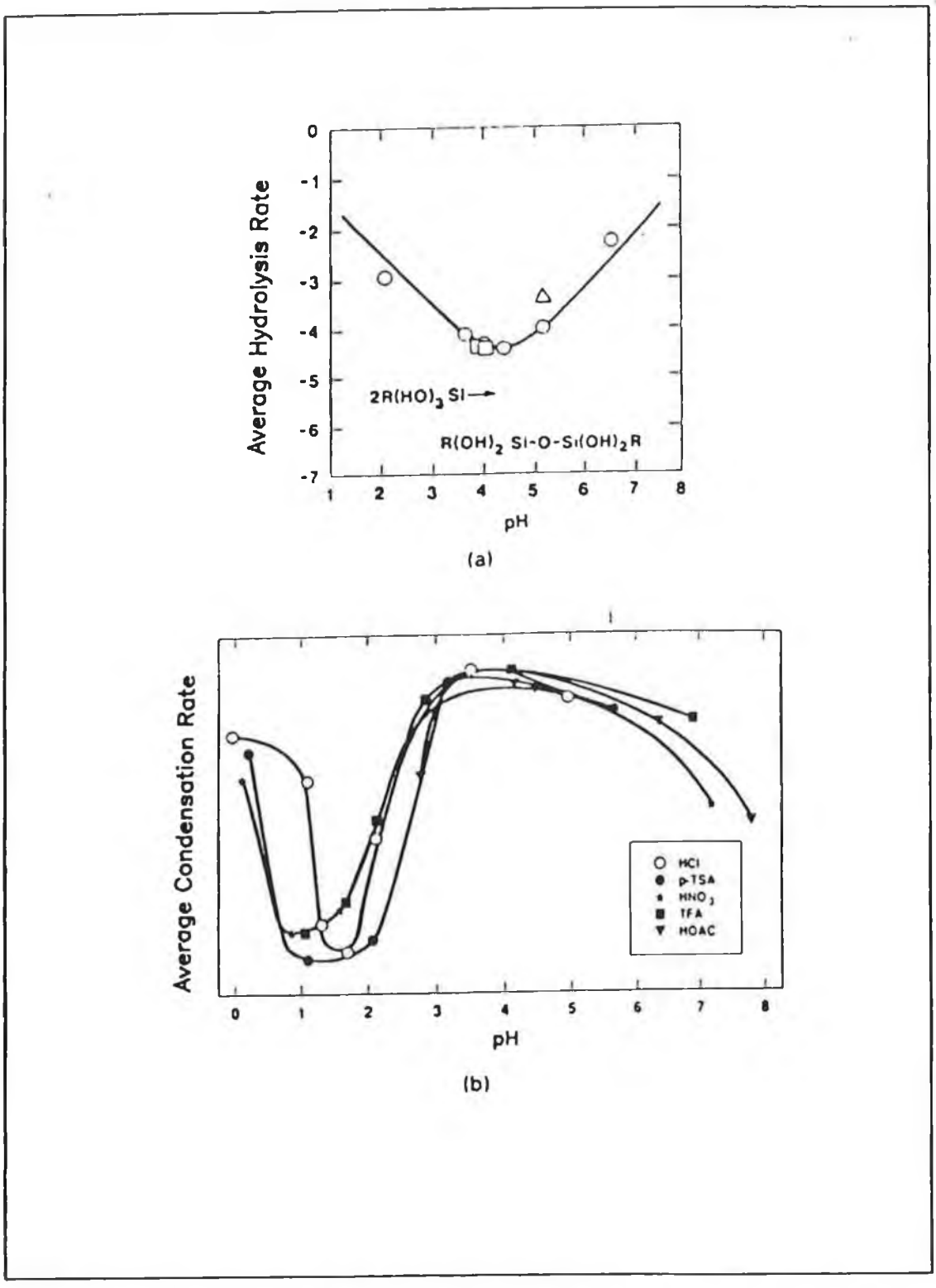

FIGURE 2.3 (a) Hydrolysis Rate as a function of pH and (b) Condensation rate as a function of pH.

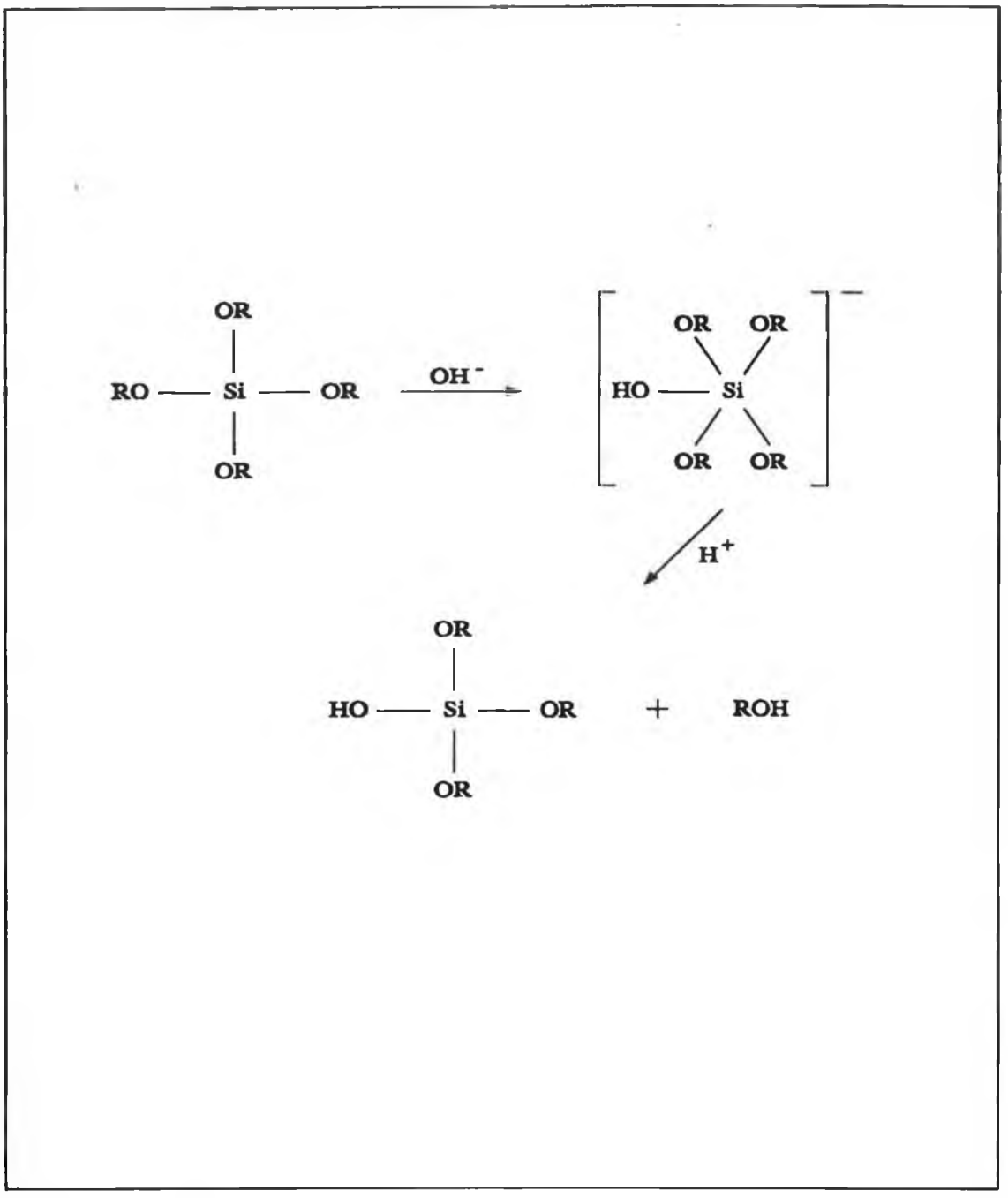

FIGURE 2.4 Five Coordinate Intermediate in the hydrolysis reaction.

Increasing the r ratio (moles H_2O/ moles TEOS) also increases the hydrolysis rate[5]. As shown in figure 2.4 the method for hydrolysis is firstly addition of OH^- to form a five ligand coordinated intermediate about the Si. Bulky ligands hinder OH^- attack

and stabilise the intermediate, thus slowing down the rate of reaction. As a general rule the bulkier the alkoxide group the slower the reaction rate.

A typical sequence of condensation products of aqueous silicates at high pH is monomer, dimer, linear trimer, cyclic trimer, cyclic tetramer and a higher order generation of colloidal particles which are commonly observed in aqueous solutions[6]. The hydrolysis and condensation reactions take place simultaneously. The presence of H_3O^+ in the solution increases the rate of hydrolysis whereas OH^- ions increase the condensation reaction[1].

2.4 Gelation

The gelation point of any system, including sol-gel silica, is easy to observe qualitatively and easy to define in abstract terms but extremely difficult to measure analytically. As the sol particles grow and collide, condensation occurs and macroparticles form. The sol becomes a gel when it can support a stress elastically. This is defined as the gelation point and the time taken to reach this point is the gelation time τ_{gel}. The change from sol to gel is gradual as more and more particles become interconnected. All subsequent stages of processing depend on the initial structure of the wet gel formed during gelation[5].

The sharp increase in viscosity that accompanies gelation "freezes" in the particular polymer structure at the gel point. At this point gelation may be considered as a rapid solidification process. The "frozen in" structure may change appreciably with time, depending on temperature and pH conditions or on the process of solvent removal[7]. In general base-catalysed sols develop a colloidal structure while, in contrast, the acid catalysed systems are characterised by highly branched structures[8]. Gels manufactured by hydrolysis and condensation of TEOS with a small amount of H_2O of pH less than 2 are made up of primary particles of about 1.0nm in diameter that associate in chain-like clusters, giving an average pore size of 6.0 nm. The particles of the base catalysed hydrolysis and condensation reaction tend to associate in larger clusters[5].

2.5 Aging.

The structural properties of a wet gel continue to change long after the gel point. This

process is called aging. The aged gel is less likely to crack than a gel which does not undergo the aging process.

2.6 Drying

There are three stages of drying. During stage 1 of drying the decrease in the volume of the gel is equal to the volume of liquid lost by evaporation. The compliant gel network is deformed by the large capillary forces which cause shrinkage of the object. Stage 1 ends and stage 2 begins when the "critical point" is reached. Classical drying theory calls this the "leatherhard point". The critical point occurs when the strength of the network has increased sufficiently to resist further shrinkage, due to greater packing strength of the solid phase. This condition creates the highest capillary pressure and the pores, unable to compress the gel any further, begin to empty, which is the start of stage 2. In stage 2 pore liquid, driven by a gradient in capillary stress, flows to the surface where evaporation takes place. This gradient capillary stress is a major contributor to fractures within the drying gel due to high stresses and low strain tolerances of the material. Stage 3 of drying is reached when the pores have substantially emptied and surface films along the pores cannot be manufactured. The remaining pore liquid evaporates in the pores and diffuses to the surface. There are no further dimensional changes, just a slow progressive loss of weight until equilibrium is reached.

2.7 Stabilisation

Both thermal and chemical stabilisation are required for the material to be used in an ambient environment. The reason for the stabilisation treatment is the very large concentration of silanols on the surface of the pores of these large surface area materials.

Chemical stabilisation involves reduction of the concentration of surface silanols below a critical level so that the surface does not re-hydroxylate in use. Thermal stabilization involves sufficent surface area reduction to enable the material to be used at a given temperature without reversible structural changes. The mechanisms of thermal and chemical stabilization are interrelated because of the extreme effects that surface silanols and chemisorbed water have on structural changes. In fact, full

densification of the silica gels, transforming them to a transparent glass is nearly impossible without dehydration of the surface prior to closure. To achieve dehydration it is necessary to recognise that "water" is present in two forms: free water within the ultraporous gel structure (i.e. physisorbed water) and hydroxyl groups associated with the gel surface (i.e. chemisorbed water). The physisorbed water can be eliminated and surface silanol (Si-OH) groups condensed starting at about 170°C. The dehydration is completely reversible up to 400°C. Above 400°C the dehydration process is irreversible as a result of shrinkage and sintering. Therefore, the concentration of existing hydroxy groups on the gel surface is an inverse function of the temperature of densification. Viscous flow occurs above 850°C with the exact temperature depending on the pore size and the specific gel. The isolated hydroxyl groups on the gel surface react with each other, bringing particles together, thereby eliminating voids within the gel. If surface H_2O is unable to be desorbed prior to pore closure it is trapped inside the densified gel.

2.8 Densification

Densification is the final process. As indicated in fig 2.1, densification of a gel network occurs between 1000 and 1700°C depending on the radii of the pores and the surface area. The amount of water in a gel has a major importance in the sintering behaviour. For example, a gel prepared by acidic conditions has a higher surface area and water content than a gel prepared in basic conditions and starts to densify at a lower temperature than the base catalysed gel[9]. During sintering the driving force is a reduction in surface area [10]. The structural evolution during the gel-to-glass conversion is difficult to quantify in absolute terms because there is no definite structure of a gel [5].

2.9 Summary

This chapter served as a guide to the sol-gel process. The stages of the process were explained and defined. The various stages of production discussed here will be referred to in the results which will follow.

CHAPTER 3

FLUORESCENCE SPECTROSCOPY

3.1 Introduction

The spectroscopy of the ion probes used in this work is discussed in this chapter. An introduction to electronic energy levels and the associated absorption and fluorescence transitions is provided.

3.2 Absorption and Fluorescence Transitions

Fluorescence emission involves radiative transitions between electronic energy levels of a material and the emission is characteristic of the material. The fundamental excitation and emission processes are illustrated in the generalised energy level diagram shown in figure 3.1.

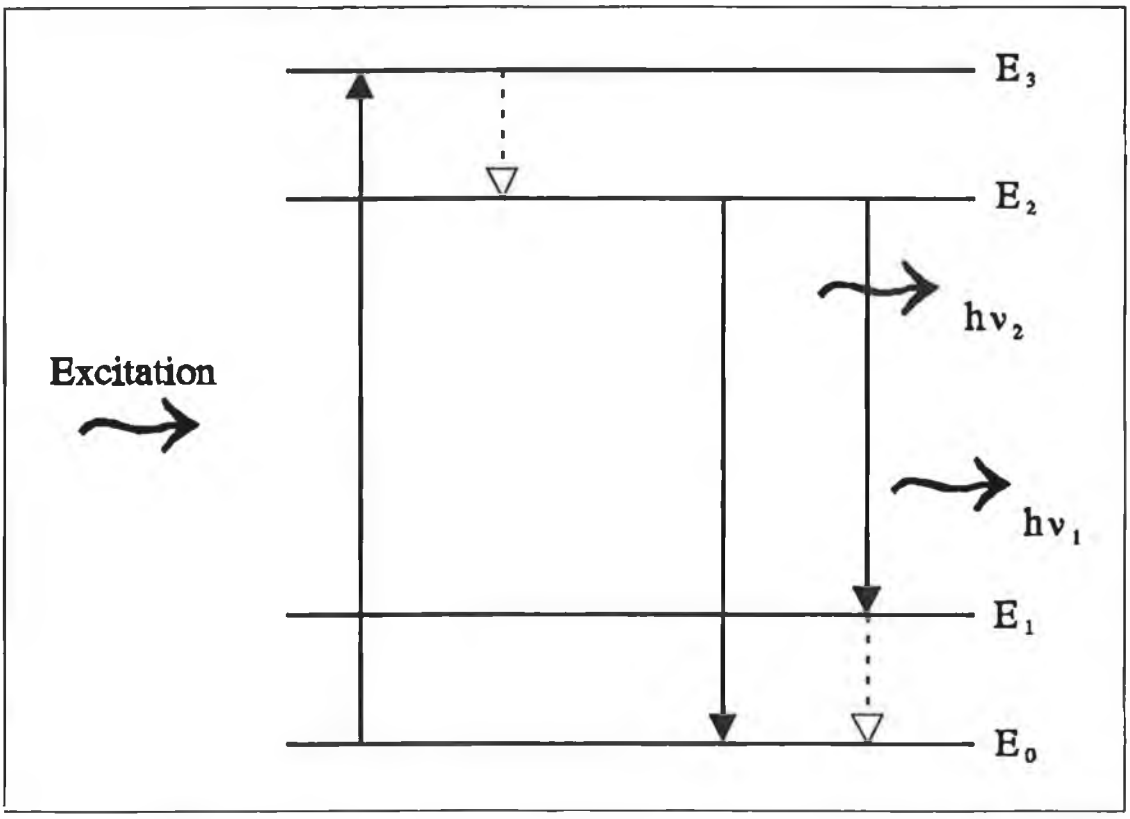

FIGURE 3.1 Excitation and Decay by Photon Emission in an Optically Active Material

The ground state has energy E_0, while E_1 E_2, and E_3 represent energies of excited states. The material is raised to excited state E_3 by electromagnetic radiation, electron collisions or a chemical reaction. If the gap between E_3 and E_2 is small, the electron in that excited state tends to decay non-radiatively by phonon emission, releasing energy as heat to the material. Radiative decay only occurs when the gap to the adjacent lower level is above a critical value. Consequently when the electron is excited to the E_3 level, it loses energy as heat by deexciting to E_2. The material decays radiatively from level 2 emitting a photon and ending on level 1 or 0. If the material decays radiatively to state 1 it then decays non-radiatively through the small gap to the ground state. In figure 3.1. the emission can be described as

$$h\nu_1 = E_2\text{-}E_1 \qquad (3.1)$$

$$h\nu_2 = E_2\text{-}E_0 \qquad (3.2)$$

where ν is the frequency of the radiation and h is Plancks constant.

3.3 Nature of Fluorescent Materials

Inorganic fluorescent solids are either large band gap semiconductors or insulators, since both of these are characterised by a filled electron band separated by a sufficiently large gap from an adjacent unfilled electron band. In the case of an insulator, the band gap corresponds to the energy of an ultraviolet photon and visible fluorescence is not expected from the pure material. Impurity atoms, however, are always present and these may possess electronic energy levels separated by a gap which corresponds to a photon of visible light. The fluorescence from insulators is almost always associated with such impurity atoms [1]. Deliberate incorporation of these impurities into an insulator provides a matrix probe, the fluorescence of which will change as a function of changes in the matrix.

3.4 Electron Energy Levels

The energy levels associated with an ion in a solid are derived from the total energy of the ion's electrons. The electronic state is described by the quantum numbers n, l, m_l, m_s, where n is the principal quantum number, l denotes orbital angular momentum, m_l is the magnetic orbital quantum number which can have values $-l$, $-(l-1)$, ...0.....$+l$, and m_s is the spin quantum number with values $\pm$ 1/2. In a

solid the orbital and spin angular momenta may interact under different coupling schemes. In general individual *l* values couple to give total angular momentum L and individual spins couple to give total spin S. The allowed values of L are labelled as follows:

L =	0	1	2	3	4	5	6	7	8
Symbol=	S	P	D	F	G	H	I	K	L

Finally L and S couple to give total angular momentum J, which results from vectorial combination of L and S[2]. This Russell-Saunders or LS coupling is illustrated in figure 3.2 for an ion with d^2 configuration. Hence, any spectroscopic state can be symbolically described with the lower right hand subscript denoting the value of the total quantum number J and the upper left hand superscript denoting the multiplicity which has a value of 2S+1, (where S is the resultant spin quantum number). As an example, an electronic state with S=2, L=3 and J=0 is denoted by $^5F_0$.

3.5 Electronic Spectra

When an optically active ion is placed in a solid, the manner in which it interacts with electromagnetic radiation is governed by the initial and final energy states of that ion and how strongly that ion interacts with the solid. If a flux of photons N is incident on an active medium of thickness d then

$$\frac{\delta N}{\delta x} = - Nk \qquad (3.3)$$

where k is the probability of photon absorption per meter and the thickness, d is measured along the x axis.

On integrating:

$$\int_{N_{x=0}}^{N_{x=d}} \frac{\delta N}{N} = - k \int_{x=0}^{x=d} \delta x \Rightarrow \ln \frac{N_d}{N_o} = - kd \qquad (3.4)$$

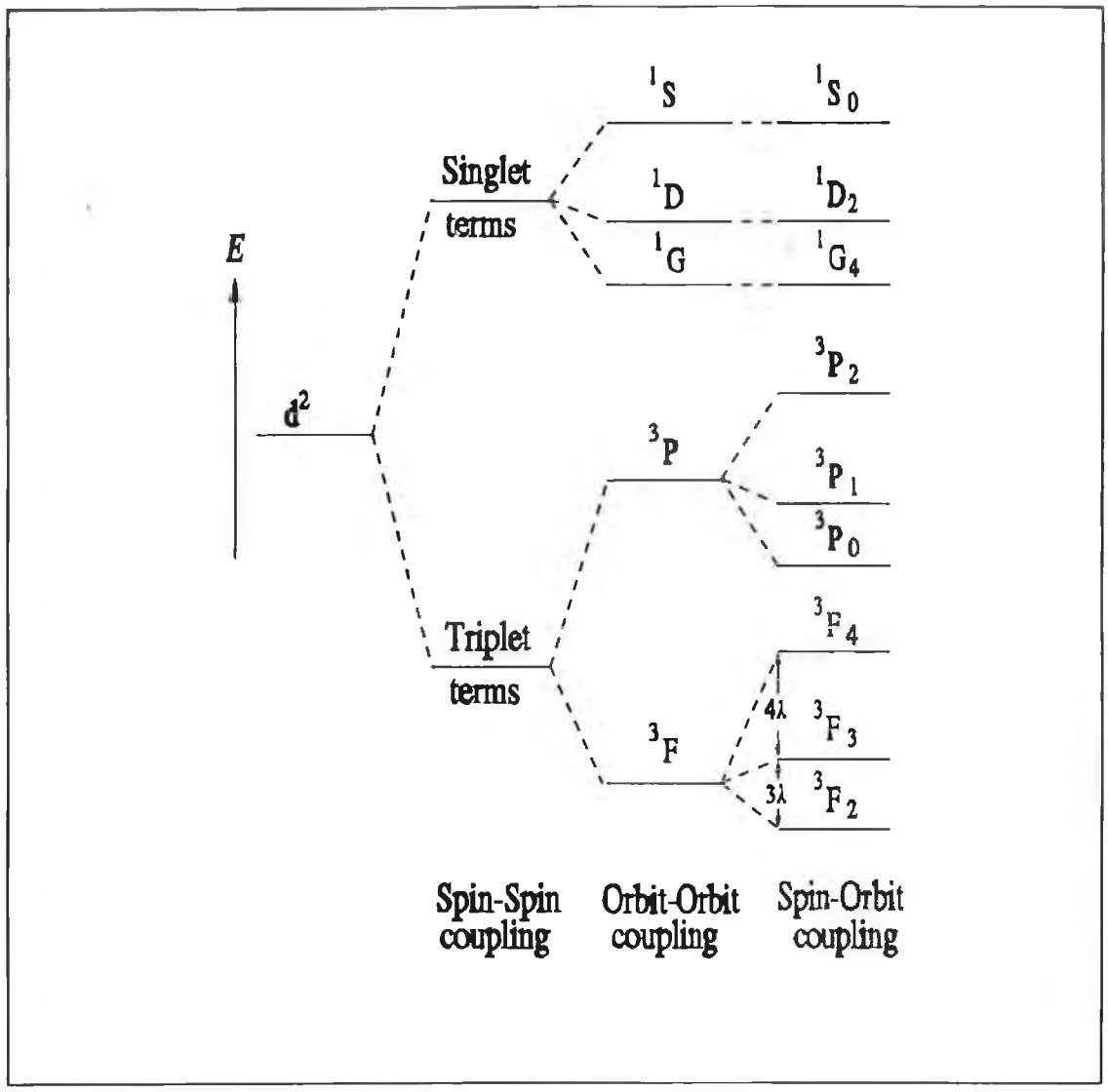

FIGURE 3.2 Splitting of Energy Levels due to Coupling

The intensity of light I_o is proportional to N_o [1] so

$$\ln\frac{I_d}{I_o} = -kd \qquad (3.5)$$

The value of k is called the absorption coefficent of the solid. Not all the theoretically possible electronic transitions are actually observed. A formal set of selection rules exists which distinguishes between "allowed" and "forbidden" transitions. "Allowed" transitions occur commonly. "Forbidden" transitions do occur but much less frequently, and they are consequently of much lower intensity[2]. The selection rules

are determined from the transition probability discussed below.

Electromagnetic radiation can interact with an optically active ion through the electric field of radiation (electric dipole process) or the magnetic field of radiation (magnetic dipole process). In general allowed transitions are electric dipole transitions and forbidden transitions are magnetic dipole in nature. The magnetic dipole process is a weaker process than the electric dipole process and hence yields a lower absorption or emission coefficient, . The probability of either a magnetic or electric dipole transition occurring is governed by the relationship

$$P_{if} = \left(\frac{2\pi}{\hbar}\right) V_{fi}^2 \, \delta(E_i - E_f - h\omega) \qquad (3.6)$$

where E_i is the initial energy of the system and E_f is the final energy. V_{fi} is the appropriate matrix element of the Hamiltonian operator **V**, denoting the interaction energy between the electron and the electromagnetic wave. (bold print denotes vector quantities). For an electric dipole transition, V=**p.E** where **p** is the electric dipole moment of the electron and **E** is the electric field intensity of the incident radiation. For a magnetic dipole transition the interaction the interaction term is V=**μ.B**, where **μ** is the magnetic dipole moment and **B** is the magnetic field strength of the radiation field[1].

Any electronic transition which involves a change in the orbital angular momentum quantum number $\Delta l = \pm 1$ is "Laporte allowed" or parity allowed, and therefore such transitions have a high probability of absorption and emission. If there is no change in the quantum number, i.e. $\Delta l = 0$ then these "Laporte forbidden" transitions have an absorption coefficent of 10^3 less than the allowed transitions. This rule may be relaxed in an unsymmetrical environment where similar orbitals have different near neighbours and hence different energy. For example, as Cr^{3+} is in a trigonal crystal field environment in Al_2O_3 the Δl=0 selection rule is relaxed giving rise to the partially allowed electric dipole laser transition , while in MgO, Cr^{3+} is in a cubic environment and the emission is a weak magnetic dipole transition.

During a spin allowed transition an electron does not change its spin, i.e. ΔS=0. Molar absorption coefficent, ε, is the product of the absorption coefficent and the

TABLE 3.1 Molar Absorption Coefficients (ε) for Different Types of Transitions

TYPE OF TRANSITION	TYPICAL VALUE OF ε
Spin forbidden, Parity forbidden	0.1
Spin allowed, Parity forbidden	10
Spin allowed Parity "partially allowed" by orbital mixing	5×10^2
Spin allowed, Parity allowed	10^4

molecular weight of the absorbing substance. Table 3.1 explains how the molar absorption coefficient changes with the allowed/forbidden transitions[2].

3.6 Radiative and Non Radiative Transitions

Many of the fluorescent ions in solid/glass environments have quantum efficiencies far below the theoretical limit of 1, indicating a decay process other than photon emission. It is therefore assumed that there exists a coupling mechanism between the excited ion and the host matrix which allows an energy transition between the ion and the host. This is achieved through phonon-assisted decay. If the energy gap between an excited level and an adjacent lower level is small, the material in that excited state tends to decay non-radiatively (by phonon emission) releasing the energy as heat to the material.

3.7 Optically Active Ions.

Any ion which absorbs optical radiation in the visible region of the spectrum is termed optically active. One such optically active ion is Cr^{3+}. When Cr^{3+} is incorporated into an insulator the material is coloured. In the case of aluminium oxide (Al_2O_3) the colour is pink and this occurs because Cr^{3+} absorbs strongly in the blue and green regions of the spectrum. Indeed the colour of ruby may vary from pink to red depending in the Cr^{3+} concentration. Cr^{3+} in glass gives the glass a green colour, which indicates that the environment of the host matrix plays a big role in determining the emission characteristics of the dopant ion. In a symmetrical crystal environment

Eu^{3+} displays characteristic f-f narrow transitions, while Eu^{3+} in a glass structure has broader peaks with some splitting of degeneracies. As stated earlier, doping of a glass with an optically active ion should make possible some qualitative/quantitative structural elucidation of the ion's environment by examination of the optical properties of the ion. Optical probes studied for this research project are Eu^{3+}, Cr^{3+}, and UO_2^{2+}.

3.8 Europium as a Fluorescent Probe

The fluorescence of the Eu^{3+} ion was exploited to elucidate the nature of the sol-to-gel transition in Silica gels. UO_2^{2+} was also codoped with Eu^{3+} to act as an excitation source for Eu^{3+}. The Eu^{3+} ion which has a configuration $4f^6$, $5s^2$, $5p^6$, has strong f-f emission transitions in the visible. Each of these electronic transitions which are shown in figure 3.3 can be used to provide information on the ionic environment.x (i) The $^5D_0$ - $^7F_0$ transition has a degeneracy of one (2J+1)when J=0, while the transitions to J=1 and J=2 have degeneracies of 3 and 5, respectively. The nature of the ion environment largely determines whether or not these degeneracies are split and hence determines the number of resolved transitions observed. The $^5D_0$-$^7F_0$ singlet transition cannot be split by the matrix environment. The line width is a result of the inhomogeneous broadening induced by a large collection of different sites made available to the ion in the glass environment. Because there exists such a range of sites the transition width can be used as an indicator of the symmetry of the surroundings in which the ion resides. (ii)The $^5D_0$ - $^7F_1$ transition is magnetic dipole in nature and is not significantly influenced by the environment surrounding the Eu^{3+} ion. Hence the transition probability at room temperature is approximately constant for all environments[3]. The measured intensity of this emission peak can be therefore used to normalise spectra for cross-referencing. (iii)The $^5D_0$-$^7F_2$ transition is partly electric dipole in nature and responds to changes in the environment. In order for a Laporte forbidden transition to occur in the 4f shell, an asymmetric environment is required, altering the parity of the orbital and allowing the transition. The greater the degree of asymmetry, the more probable the transition, and the more intense the corresponding spectral peak becomes. In an attempt to quantify the asymmetry dependence of the emission intensity, the ratio of the intensity of the two transitions

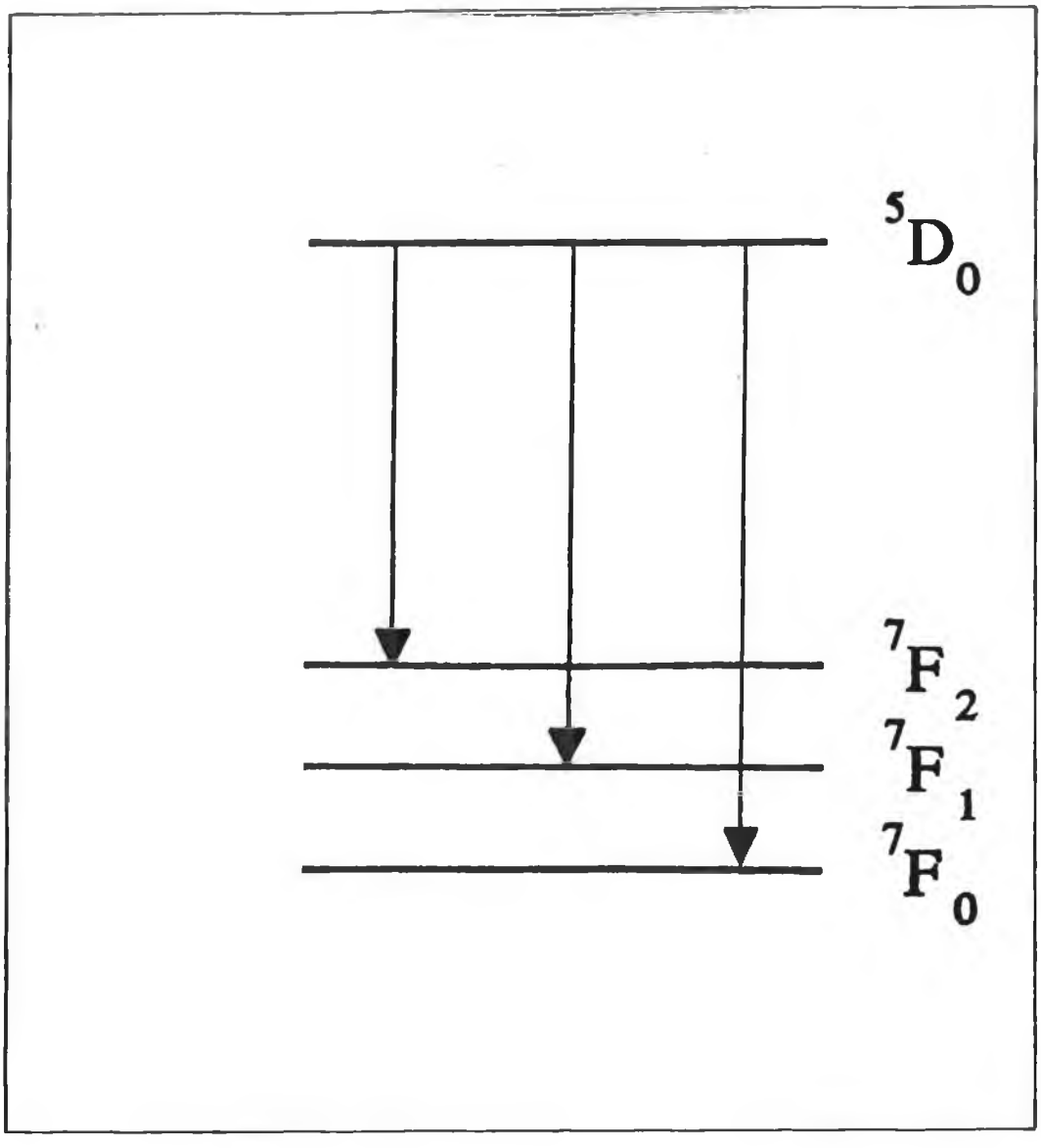

FIGURE 3.3 Eu^{3+} Transitions

$^5D_0$ - $^7F_2$ and $^5D_0$ - $^7F_1$ is used. This ratio, the fluorescence ratio, denoted R_{FL} is given by

$$R_{FL} = \frac{I_{(^5D_0-^7F_2)}}{I_{(^5D_0-^7F_1)}} \qquad (3.7)$$

3.9 Chromium as a Fluorescence Probe

The orbitals of loosely bound d electrons of the Cr^{3+} ion are very sensitive to changes in the ion's environment. Transition metals will occupy tetrahedral or octahedral sites

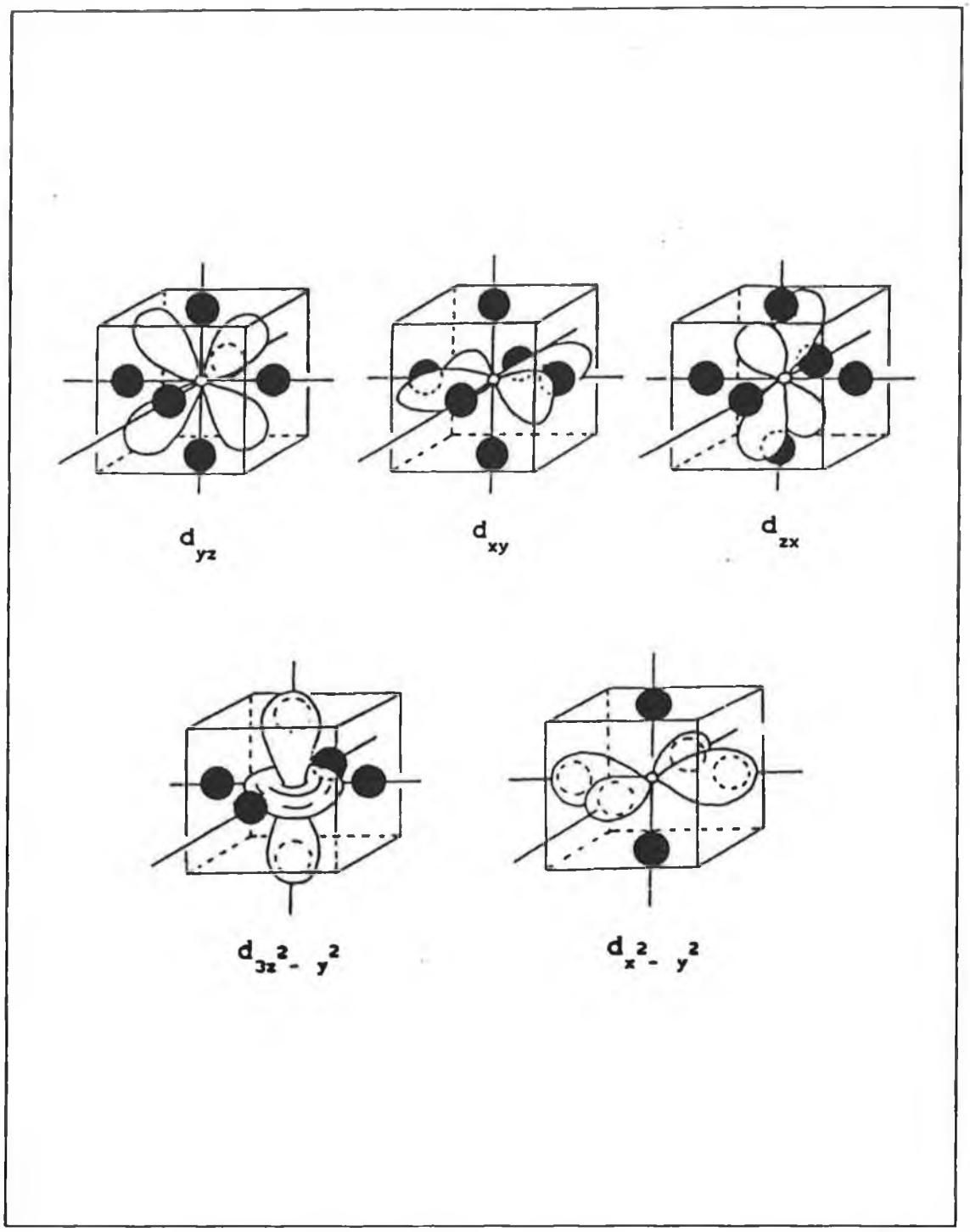

FIGURE 3.4 Transition metal ion in a Ligand Field

in a structure depending on availability and electronic configuration. Oxide crystals are particularly suitable as hosts, and when the six surrounding oxygens (in the octahedral case) are equidistant from the ion, the ion is in a site of perfect octahedral

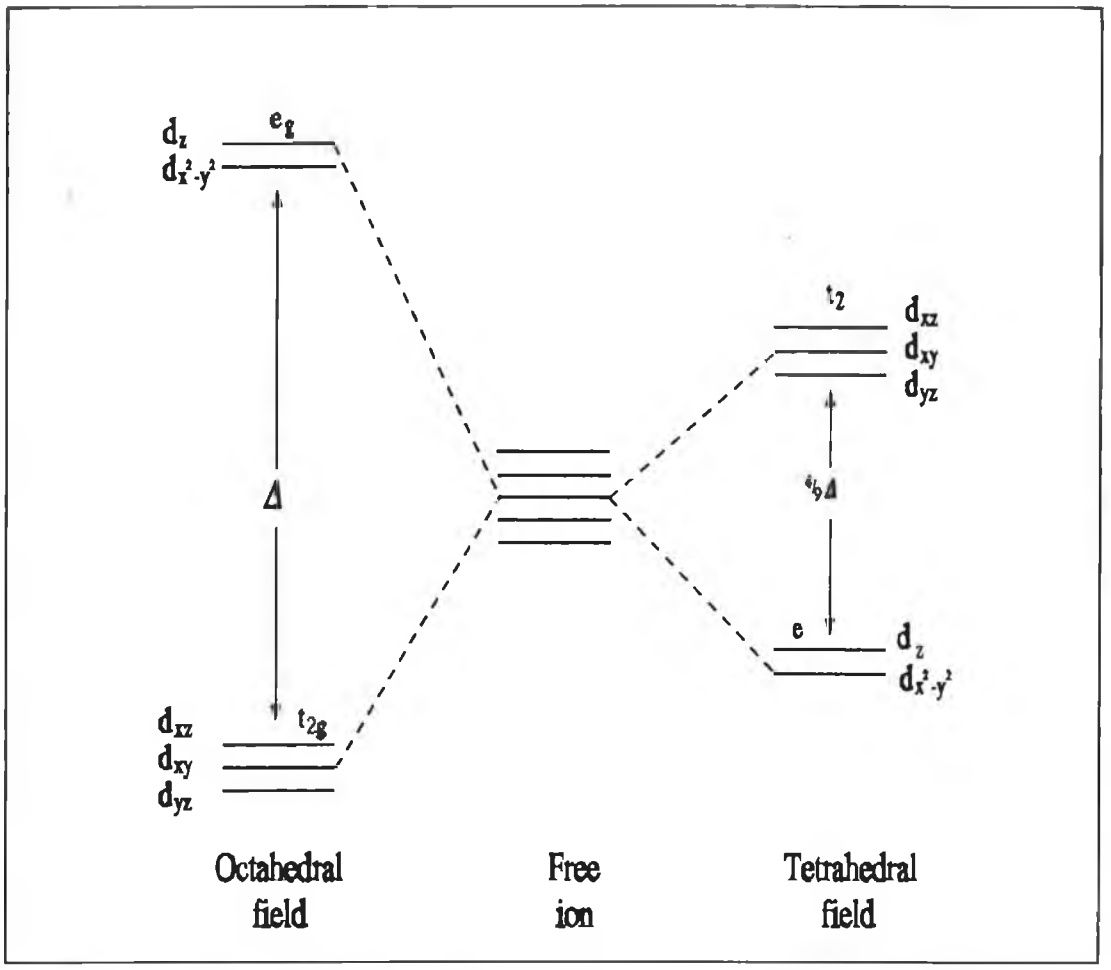

FIGURE 3.5 d Orbital Splitting in Ligand Fields

symmetry. In many oxide hosts the arrangement of the six oxygen ions is distorted from the perfect octahedral symmetry and this distortion results in a splitting of the d orbital energy. The shapes of these five d orbitals are shown in Figure 3.4, where the ion is surrounded octahedrally by six oxygen atoms.

The d_{xy}, d_{yz}, and d_{xz} are affected in a similar way by the oxygen ions; as a result these orbitals have the same energy and are labelled t_{2g}. The d_z^2 and the d_{x2-y2} have lobes which point towards the oxygen ions thus giving a higher interaction energy between the O^- and any occupying electron. These orbitals have higher energy and are termed e_g orbitals. The d_z^2 and the d_{x2-y2} have the same energy which is larger than that of the other three orbitals [2]. The orbital energy split in a tetrahedral field is exactly opposite in that the t_{2g} orbitals have the highest repulsion and therefore the highest

energy. The d orbital split in a tetrahedral and octahedral field is shown in figure. 3.5. Cr^{3+} is a d^3 ion and has been found to occupy distorted octahedral sites in the SiO_2 structure. The electronic energy levels of Cr^{3+} in an octahedral ligand field are presented in Figure 3.6 [4], In this diagram the energy level labelling is derived from group theory. The principal absorption transitions are $^4A_2$-$^4T_2$ and $^4A_2$-$^4T_1$ while the fluorescence transitions are ^2E-$^4A_2$,$^2T_2$-$^4A_2$ and$^4T_2$-$^4A_2$. The $^4A_2$-$^4T_2$ absorption transition at about 600nm has been observed to vary as a function of the Cr^{3+} ligand field [5]. A broadening of the $^4T_2$ absorption band indicates an increase of disorder of the ion matrix.

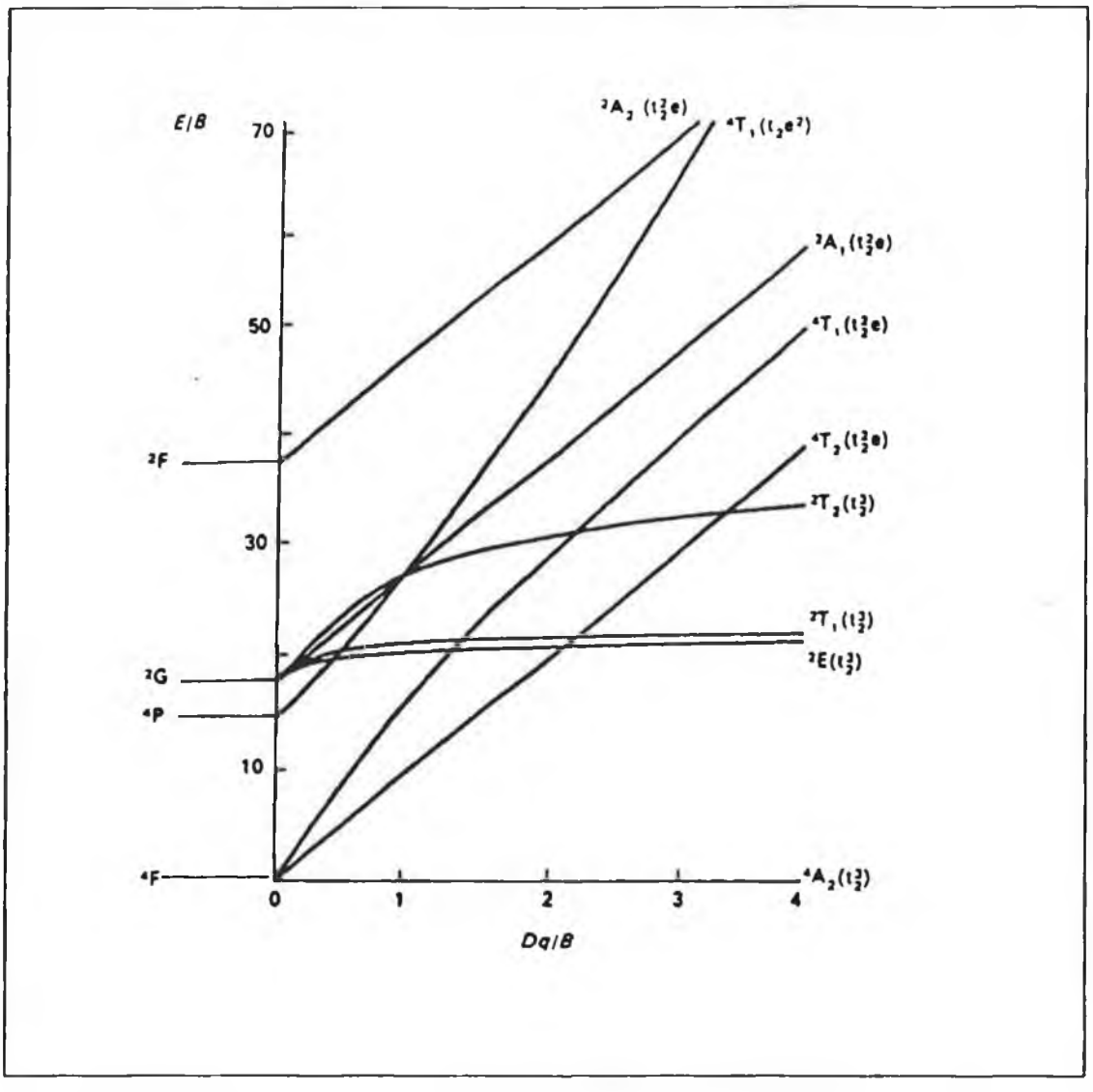

FIGURE 3.6 Energy Levels of a d^3 System in an Octahedral Field

3.10 UO_2^{2+} as a Fluorescent Probe.

The electronic energy levels in the UO_2^{2+} ion can be modeled as molecular orbitals using the principles of the linear combination of atomic orbitals (L.C.A.O.) as summarised below.

When two atoms which have atomic orbitals described by the wave functions $\Psi(1)$and $\Psi(2)$, form a bond, the electrons originally in the atomic orbitals now occupy molecular orbitals. The molecular orbital is formed by a linear combination of the atomic orbitals $\Psi(1)$and $\Psi(2)$, as given by equation 3.8.

$$\psi = N[C(1)\ \psi(1) + C(2)\ \psi(2)] \qquad (3.8)$$

N is a normalising constant chosen to ensure that the probability of finding an electron in the whole of the space is unity and C(1) and C(2) are constants chosen to give a minimum energy for ψ. Two combinations are possible in the diatomic case:

1. Where the signs of the two wavefunctions are the same.
2. Where the signs of the two wavefunctions are different.

The resulting combinations are

$$\psi(g) = N[\psi(1) + \psi(2)] \quad (Bonding\ M.O.) \qquad (3.9)$$

$$\psi(u) = N[\psi(1) - \psi(2)] \quad (Antibonding\ M.O.) \qquad (3.10)$$

$\psi(g)$ and $\psi(u)$ are the resultant molecular orbitals. Since orbitals may not be destroyed the number of molecular orbitals evolved must equal the number of atomic orbitals combined[2].

As seen in figure 3.7 atomic orbitals which overlap in the plane of the molecule form strong σ bonds and lower energy even or gerade (g) molecular orbitals. Orbitals which bond in the plane perpendicular to the plane of the molecule associate by delocalisation of electric charge mutually shared by the orbitals. As a result they form

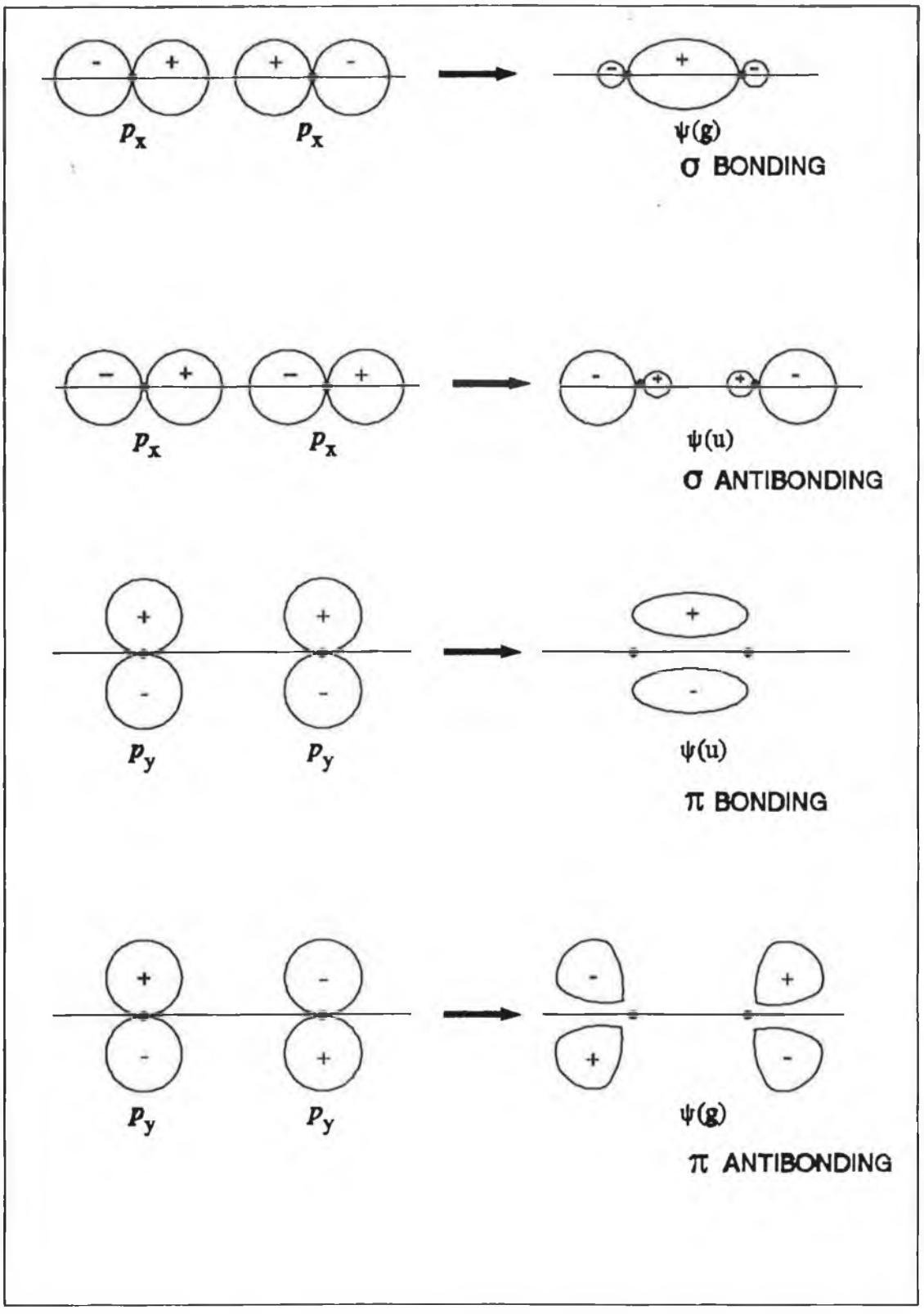

FIGURE 3.7 Atomic orbital combinations and the resulting molecular orbitals

weaker π bonds, and higher energy ungerade (u) molecular orbitals. This π electron cloud perpendicular to the plane of the molecule causes a large electrostatic repulsion in that direction. Empty orbitals stay associated with the parent atom at an energy level greater than that of the molecular orbitals.

The UO_2^{2+} ion is a linear molecule containing two U-O sigma bonds and two U-O π bonds. The unoccupied f orbitals remain associated with the uranium atom, while the occupied orbitals combine with the Oxygen p orbitals to form a complex molecular orbital energy system. Electron excitation in the region of 400nm excites a transition from two molecular orbitals (of type π_u consisting almost exclusively of oxygen 2p in the L.C.A.O. model) to the empty 5f shell of the uranium atom. This charge transfer type transition is parity allowed. The fluorescence spectrum of UO_2^{2+} varies from a series of roughly equidistant narrow bands as found in silicate or phosphate glasses to a broad structure similar to that found in octahedral perovskites and in germanate glass[6]. The existence of vibrational energy levels associated with the UO_2^{2+} molecule manifests itself as a number of peaks in the fluorescence spectrum. The separation of these vibrational spectral peaks reflects the relative coupling of molecular vibrational modes and hence the position of the surrounding ligands. The decay time of the ion also varies with structure.

3.11 Summary

The spectroscopy of the ion probes used was discussed in this chapter. An introduction to electronic energy levels and the associated absorption and fluorescence transitions was provided. It is clear that the spectroscopy of these probes can be used to investigate the structure of the ionic environment.

CHAPTER 4

SOL-GEL GLASS PRODUCTION AND EXPERIMENTAL TECHNIQUES

4.1 Introduction

In this chapter the methods used to produce the materials studied are outlined. The experimental equipment used to obtain the fluorescence and lifetime data are discussed. An explanation of the data acquisition process is also provided.

4.2 Synthesis of Silica Gels

The various stages of sol-gel glass production are broadly defined as follows:

A sol is a dispersion of colloidal particles in a liquid, where a colloid is a solid particle with diameters of 1 to 100nm.

A gel is an interconnected, rigid network with pores of submicron dimensions and polymeric chains the length of which is greater than a micron.

The materials used to produce the silica glasses were high performance liquid chromatography (HPLC) grade ethanol, electronic grade 99%+ tetraethylorthosilicate (TEOS) and deionised water. The water was brought to the required pH by the addition of concentrated hydrochloric acid or sodium hydroxide. The nitrate form of the dopant ion was added in the initial stage of the process. Compounds used include europium nitrate pentahydrate ,uranyl nitrate pentahydrate, and chromium nitrate pentahydrate.

Water and TEOS require a common solvent as they are only slightly miscible in each other. Ethanol (EtOH) was used as the common solvent and the volume required relative to water increases with the pH of the reaction mixture. In general the fraction $EtOH/(EtOH+H_2O) = 0.4$ was used for acid solutions and 0.8 for basic solutions. The two pH domains used were $pH < 2$ and $2 < pH < 7$. pH=2 appears as a boundary for the polymerisation process because the point of zero charge (P.Z.C.), where the surface charge is zero, and the isoelectric point (I.E.P), where the electric mobility of the silica particles is zero, are both in the range pH=1-3. Hence sols repaired below pH=2 were termed acid catalysed and sols prepared at a pH greater than pH=2 were termed base catalysed. Samples for this work were prepared at pH 1 and pH 5. pH=7

appears as a polymerisation pH boundary because both the silica solubility and the dissociation rates are maximised at pH $\geq$ 7, and because the silica particles are appreciably ionised above pH=7 so that particle growth occurs without aggregation or gelation.

Materials were weighed on an AE model 100A analytical balance, the resolution of which is 0.1mg. The nitrate form of the dopant ion probe was dissolved in a measured quantity of deionised water. Ethanol was then added and the solution mixed vigorously. TEOS was gradually added with intermittent stirring. To prevent the TEOS from precipitating out of solution it was initially introduced one drop at a time for the first 5 to 10 drops. The rest of the measured quantity then dissolved easily. The resultant sol was removed and absorption spectroscopy carried out on a Shimadzu UV-Vis absorption spectrometer to determine possible excitation wavelengths. A small sol sample was placed in a Thor refrigerator at 0°C and the remainder left to dry in a Blue M drying oven for seven days at 73°C. When samples were dried sufficiently in the oven they were raised to the required temperature (usually 200, 500 or 800°C) at a rate of 1°C per minute and maintained at that temperature for 24 hours. On cooling all samples were stored in the Thor refrigerator at 4°C.

4.3 Optimum Ion Concentration

For this study a series of samples was prepared for each ion dopant, with ion concentrations of 0.5%, 1%,2% and 5% (as a percentage of Silicon atom concentration). These samples were investigated using fluorescence spectroscopy and lifetime analysis. The ion concentration was selected as a compromise between S/N ratio and lifetime shortening by concentration quenching. The concentration which produced a distinct signal and showed minimum concentration quenching effects was chosen.

4.4 Fluorescence Data Acquisition

The experimental system which was used for recording fluorescence spectra is shown in figure 4.1. The excitation source was a 200W Applied Photophysics water-cooled xenon arc lamp. Wavelength selection was achieved by use of a Minimate 0.25m monochromator with a slit width of 0.25mm. The excitation beam was focused onto

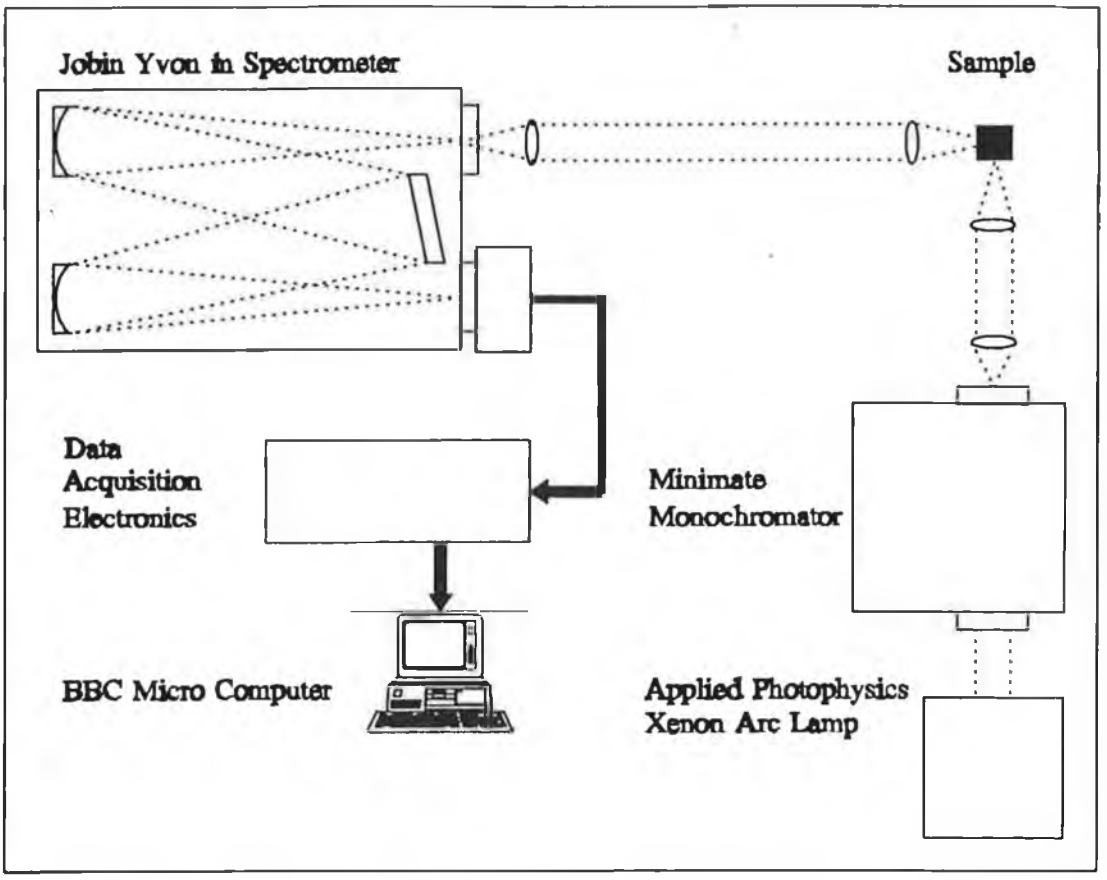

FIGURE 4.1 Experimental Arrangement for Fluorescence Data Acquisition

the sample under investigation. The resultant fluorescence was focused onto the entrance slit of a Jobin Yvon one meter focal length spectrometer. A Hamamatsu R928 photomultiplier tube was mounted on the exit slit. Other excitation sources used include a mercury ultra-Violet discharge lamp, a PRA pulsed Nitrogen laser and a He-Ne laser. The detector signal was collected by a BBC microcomputer via an Acorn electronic analogue interface board. The experimental system was controlled by a BBC Basic computer program "Aver2" written in house (see appendix 1). By using "Aver2" the operator can select the starting and finishing wavelengths and increment size. The program also carries out background signal subtraction and signal averaging, providing an improved signal to noise ratio.

4.5 Lifetime Measurement

The experimental arrangement for excited state lifetime measurement is displayed in figure 4.2. The excitation sources for this were either the PRA/Laser Photonics pulsed

nitrogen laser or the pulsed Nd:Yag laser in configuration with the Stanford Research Instruments SR400 photon counter.

The main advantage of the molecular nitrogen laser is its simplicity of operation. Operating nominally at 15kV with spark gap pressures of 45 and 80 psi, a very fast transverse excitation across a 6mm rectangular cross section channel produces a 0.6ns duration discharge, causing population inversion of the nitrogen molecules. This excited electronic state has a lifetime of about 40ns, emitting a 337nm photon on de-excitation. The involvement of vibrational sub levels in this electronic transition broadens the laser wavelength range to 30nm which makes the nitrogen laser broad band by laser standards.

The other laser source used was a Spectron 400/800 Nd:Yag Q-switched laser.

The gain in the oscillator system is provided by a population inversion among the Nd ions created by the energy input from a discharge lamp. Light is coupled from the flashlamps in the pumping chamber. The geometry of the cavity along with the uniformity of excitation of the Nd rod determines the beam quality emerging from the laser. Q-switching is made possible by a Pockels cell which consists of a Brewster-angled KDP frequency doubling crystal together with a compensating Brewster angled glass prism and military grade dielectric polariser. The laser is fitted with two harmonic generators or frequency doubling crystals for the production of green and UV light, with a harmonic separation of about 99%. It provides wavelengths at 1064nm, 532nm and 266nm. The laser power supply reference trigger is asymmetrical and incompatible with the photon counter and so a Level type 303 low noise function generator was used as an external simultaneous trigger simultaneously with the SR400 gated photon counter.

For luminescence analysis a relatively low voltage is required to minimise any chance of laser annealing of the sample. This low voltage results in an increase in the time between triggering and the laser pulse creation. A delay of 200μs is required at the A and B gates of the photon counter (discussed below) to compensate for the delay between trigger and laser pulse.

The SR400 gated photon counter provides the user with the facility to repetitively measure excited state lifetimes. The function generator, as indicated in figure 4.2, simultaneously triggers both the pulsed laser and the photon counter. The instrument

is configured to count in the "A, B for preset T" mode which means that on being enabled via a trigger pulse the counters, A and B, wait a specific time T (predetermined by the operator) before counting. The A counter counts the photon which falls within the preset gate width as the counter scans the decay as a function of time. The B counter is set to fixed delay and set to sample the emission pulse for 1ms. The count ratio A/B corresponds to a normalised intensity, overcoming any variations in the pulse intensity. The in-house software (listed in appendix 2) controlled the photon counter via an IEEE Acorn 488 board. The software saves all the important operating parameters such as gate delays, counting modes and number of triggers,as well as the data.

4.6 Lifetime Calculation

When the optically active centre is first excited it emits a maximum intensity I_0. The rate at which this intensity decreases with time is characterised by the lifetime, τ, of the excited state. The time dependence of the decay is described by

$$I = I_0 e^{-kt} \qquad (4.1)$$

Where k is the decay rate constant, and k is the inverse of the decay time i.e. $\tau = 1/k$. Hence the lifetime of an excited state can be measured as the time taken for the emitted radiation intensity to fall to 1/e of its original intensity. Rewriting equation 4.1

$$\ln I = \ln I_0 - kt \qquad (4.2)$$

indicates that a semi-logarithmic plot of lnI versus t will have a slope of -k and an intercept ln I_0. This is the procedure followed by the BBC Basic program "compstw" (Appendix 3). The program produces a weighted least squares fit of the decay curve on the computer monitor as well as a semi-log plot of the data.

Decay curves of optically active ions in glass tend to be non-exponential due to the wide variety of sites available to the ions. A common method of analysing complicated non-exponential decay curves has been described by Demas [1] and Lempicki et al. [2]. The average lifetime, τ, is defined as

$$\tau = \frac{\int tI(t)dt}{\int I(t)dt} \qquad (4.3)$$

where I(t) is the experimental decay curve. Decay curve analysis can also be carried out using a treatment based on Simpson's rule to determine the area under the curve. [3]. Both the area under the curve and the integration methods were used in the program given in appendix 3. The lifetime data in this study contain three values for each sample corresponding to the three methods used. Method 1 is the semi-logarithmic plot, method 2 is numerical integration and method 3 is based on Simpson's rule.

4.7 Summary

This chapter provided a summary of materials preparation and experimental techniques used in this work.

CHAPTER 5

Eu^{3+} AND Cr^{3+} DOPED SOL - GEL MATERIALS

5.1 Introduction

This chapter deals with the use of Eu^{3+} as a probe of the sol- gel structure. Lifetime and fluorescence data of 2% Eu^{3+} doped silica sol-gel materials are presented. A brief examination of chromium as a fluorescence probe is also undertaken.

5.2 Eu^{3+} Samples Produced for Analysis

Four sets of samples were produced according to the method discussed in section 4.2. The H_2O/TEOS ratios and pH values used in the production of these sets are summarised in table 5.1.

TABLE 5.1 Eu^{3+} samples produced for analysis

SAMPLE	r	pH
Set 1	4	1
Set 2	10	1
Set 3	4	5
Set 4	10	5

Each set consisted of a sol, a gel, and samples heated to 200°C and 800°C, respectively.

A quantity of sets 2 and 4 was taken and soaked in D_2O for 1 week before analysis.

A quantity of sample 3 gel was heated to 1400°C.

5.3 Fluorescence Studies as a Function of Drying Temperature.

Europium transitions studied in this report are detailed in figure 3.3. The $^5D_0$ - $^7F_0$ transition is observed at around 578nm, the $^5D_0$ - $^7F_1$ transition occurs at around 595nm and the $^5D_0$ - $^7F_2$ transition can be observed at about 615nm.

The fluorescence spectra as a function of drying temperature in the region of these transitions, from sample sets 1-4 are shown in Figs 5.1 - 5.4, respectively. Figure 5.2 (pH=1, r=10) is taken as a representative example of how the spectra of each set varies with temperature. The $^5D_0$ - $^7F_0$ transition at 578nm broadens on densification. This transition is matrix sensitive as discussed in section 3.8, and broadening indicates an increase in the variety of sites occupied by the Eu^{3+} ion. The relatively narrow structureless peaks of the sol are characteristic of Eu^{3+} in solution[1]. The gel spectrum is similar to that of the sol due to the large amount of water (a by-product of condensation) still present at this stage. The broadening of the spectra as the samples are dried to 200°C and 800°C, reflect the large distribution of Eu^{3+} sites in the glassy environment. At the higher temperatures, the J-splitting appears on the $^5D_0$ - $^7F_1$, and $^5D_0$ - $^7F_2$ transitions as discussed in section 3.8. This results from the increasing asymmetry of the glass matrix. The sample densified to 800°C has a fluorescence spectrum similar to Eu^{3+} in conventional glass[2]. The fluorescence ratios, R_{FL}, as discussed in section 3.8, are tabulated in tables 5.2 to 5.5. Again taking sample set 2 (pH=1, r=10) as an example, the ratios increase with densification temperature, except for a decrease between the sol and gel which will be discussed below. The increasing values of R_{FL} again reflect the increasing asymmetry of the Eu environment as the material becomes more glassy. Decay times are tabulated in tables 5.6 to 5.9. The measured fluorescence decay time τ is given by

$$1/\tau = 1/\tau_R + 1/\tau_{NR} \qquad (5.1)$$

where $1/\tau$ is the decay rate and τ_R and τ_{NR} are the radiative and non-radiative decay times respectively.

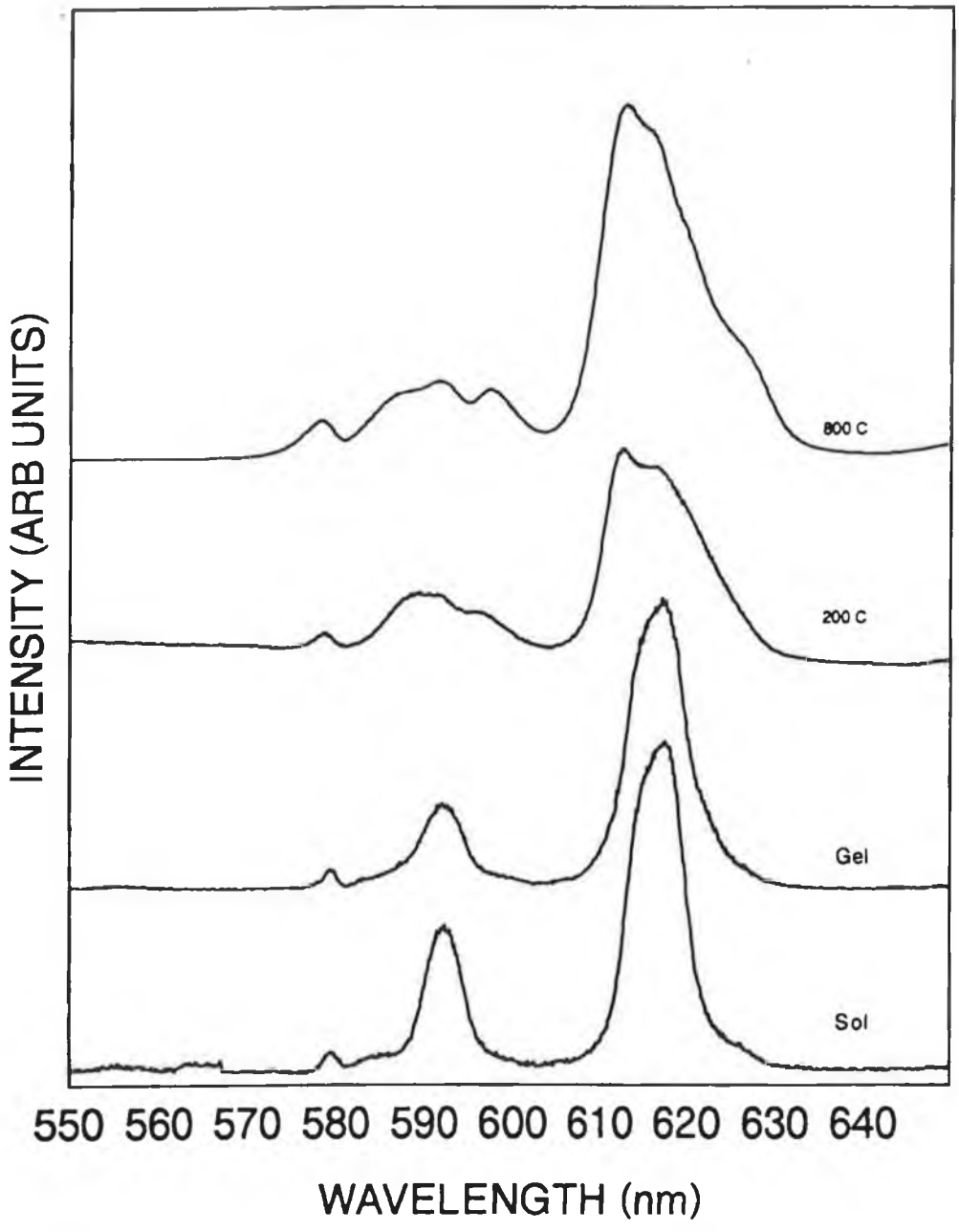

FIGURE 5.1 Fluorescence of Sample Set 1, Ph = 1, r = 4

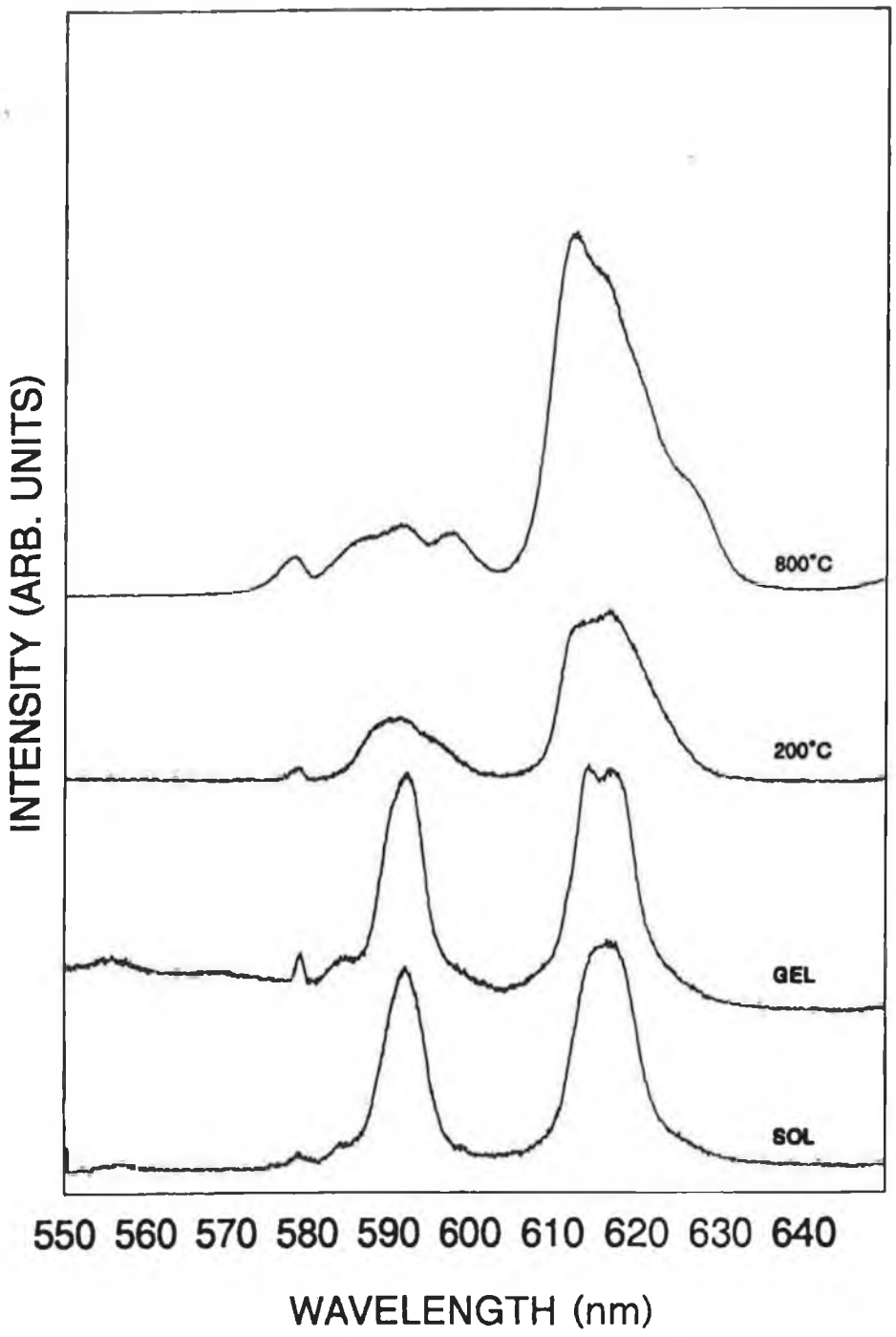

FIGURE 5.2 Fluorescence of Sample Set 2, pH = 1, r = 10

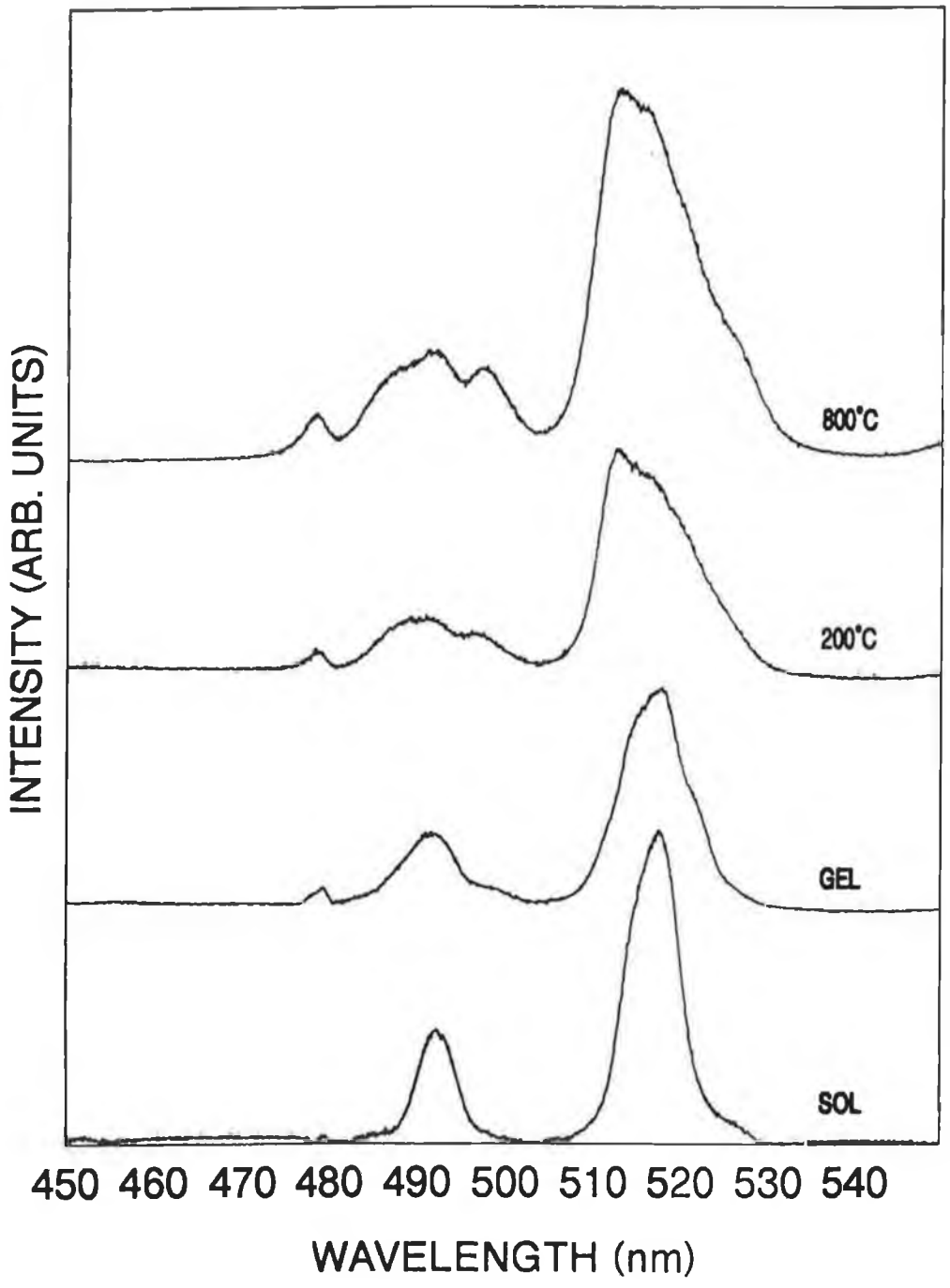

FIGURE 5.3 Fluorescence of Sample Set 3, pH = 5, r = 4

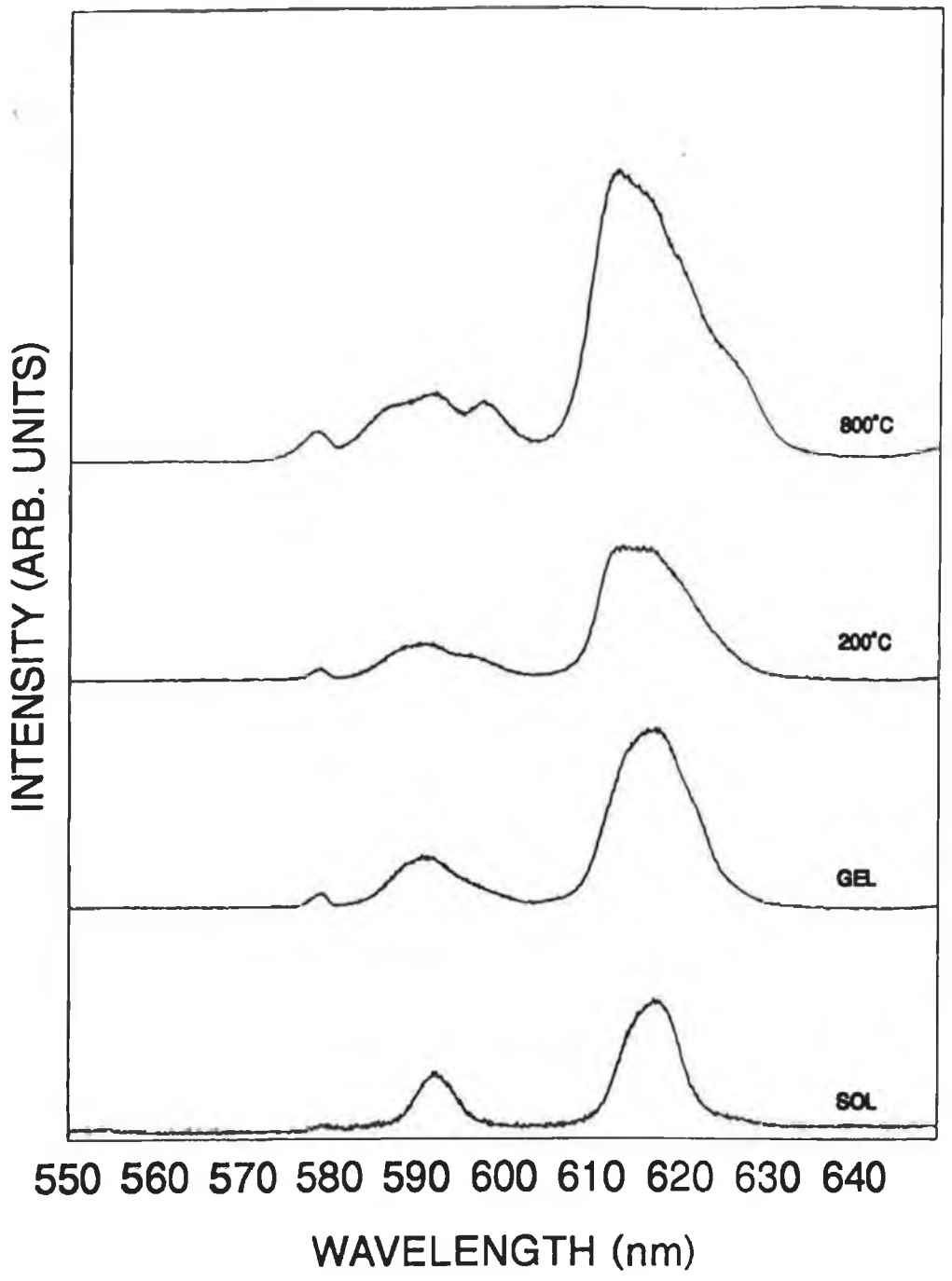

FIGURE 5.4 Fluorescence of Sample Set 4, pH = 5, r = 10

From Equation 5.1 a shorter measured decay time (τ) results from an increase in the non-radiative decay rate ($1/\tau_{NR}$). Taking table 5.7 (pH=1, r=10) as representative of the lifetime behaviour as a function of densification temperature, the sol and the gel values are low and are comparable to $\tau \approx 0.1$ms measured for Eu^{3+} in solution[1]. As the material densifies, water is removed and this is reflected in the increase in decay time measured. From equation 5.1 it is of note that both R_{FL} (Table 5.3) and τ (Table 5.7) decrease in going from sol to gel. According to equation 5.1 the gel lifetime of 0.12ms compared with the sol lifetimes of 0.14ms indicate more non-radiative decay in the gel. This would indicate an increase in the number of hydroxyl ions contributing to the non-radiative decay which is consistent with a more symmetric environment in the gel compared to the sol (increasing the number of hydroxyl ions increases the symmetry as the degree of hydroxylation increases). This model is corroborated by the parallel decrease in R_{FL}. However the effect is observed predominantly in the low pH regime and is still under investigation. From tables 5.6 to 5.9 it can be seen that the decay times for the 800°C samples are ≈ 1.2ms. This is considerably lower than the value of 2.8ms measured for the fully densified glass. Hence although the fluorescence spectra indicate that the glass environment is established by 800°C, the decay time data suggest the presence of residual hydroxyl ions in the matrix which contribute to the non-radiative decay rate of the ion.

TABLE 5.2 pH=1, r=4

SAMPLE	R_{FL} (±0.5)
Sol	2.2
Gel	3.1
200°C	3.5
800°C	5.7

TABLE 5.3 pH 1, r=10

SAMPLE	R_{FL} (± 0.5)
Sol	1.5
Gel	1.2
200°C	2.4
800°C	4.2

TABLE 5.4 pH 5, r=4

SAMPLE	R_{FL} (± 0.5)
Sol	2.8
Gel	2.8
200°C	3.4
800°C	3.6

TABLE 5.5 pH 5, r=10

SAMPLE	R_{FL} (± 0.5)
Sol	2.2
Gel	3.3
200°C	3.5
800°C	4.0

TABLE 5.6 Lifetime of sample set 1, pH = 1, r = 4

SAMPLE	METHOD 1 ms(± 0.01)	METHOD 2 ms(± 0.01)	METHOD 3 ms(± 0.01)
Sol	0.15	0.16	0.16
Gel	0.12	0.12	0.12
200°C	0.27	0.28	0.28
800°C	1.23	1.25	1.26
1400°C	2.79	2.81	2.83

TABLE 5.7 Lifetimes of Sample Set 2, pH = 1, r = 10

SAMPLE	METHOD 1 ms(± 0.01)	METHOD 2 ms(± 0.01)	METHOD 3 ms(± 0.01)
Sol	0.14	0.15	0.16
Gel	0.12	0.12	0.13
200°	0.29	0.30	0.34
800°C	1.25	1.27	1.30

Hydroxyl ions bonded to silicon on the pore surface also make a contribution. The D_2O soaking experiments discussed in a later section attempt to investigate the contribution of hydroxyl ions to the quenching of the fluorescence and the decrease in decay times.

5.4 Fluorescence Studies as a Function of pH

Taking figures 5.2 and 5.4 and tables 5.3 and 5.5 as representative of the two pH regions the principal feature is the smaller value of R_{FL} for the pH=1 material compared to the pH=5 material. Acid conditions increase the hydrolysis rate while

TABLE 5.8 Lifetime Measurements for Sample Set 3, pH = 5, r = 4

SAMPLE	METHOD 1 ms(± 0.01)	METHOD 2 ms(± 0.01)	METHOD 3 ms(± 0.01)
Sol	0.18	0.19	0.19
Gel	0.15	0.17	0.17
200°C	0.29	0.30	0.31
800°C	1.26	1.26	1.30

TABLE 5.9 Lifetime measurements for Sample Set 4, pH = 5. r = 10

SAMPLE	METHOD 1 ms(± 0.01)	METHOD 2 ms(± 0.01)	METHOD 3 ms(± 0.01)
Sol	0.15	0.15	0.16
Gel	0.14	0.14	0.14
200°C	0.23	0.23	0.24
800°C	1.26	1.25	1.30

the condensation rate is relatively slow, as discussed in section 2.3. As a result of this there is more water present in the pH=1 environment compared to the pH=5. These conditions provide a more symmetrical environment for Eu^{3+} at pH=1 which is consistent with the R_{FL} values in this regime. The decay time data in tables 5.6 to 5.9 corroborate this behaviour, in so far as the trend is for a shorter lifetime at the lower pH both for r=4 and r=10.

The 200°C and 800°C data show similar trends in both pH regimes. It is expected that the pH effect will be minimised as the samples are densified to a higher temperature. However, the initial pH conditions in the sol strongly influence the structural evolution of the materials. At low pH the gel is expected to be a highly ramified chain-like structure. When dried, these gels are highly porous and have a large surface area with

pore sizes of the order of nm[3]. In this environment the Eu^{3+} is exposed to the water and organics at the early stages of the process, thus resulting in a low fluorescence ratio and shorter decay time as found in this study. At the higher pH, the structure is more colloidal and it is likely that the Eu^{3+} ion is more shielded from the aqueous environment of the sol and the gel. Furthermore, hydrolysis rates are slower relative to the condensation rate and so there is less water in the materials. This model is corroborated by the pH=5 data where both R_{fl} values and decay times are higher. For r=10, in the high pH regime the decay times are lower than expected according to the model. This is discussed in the next section.

5.5 Fluorescence Studies as a Function of r

The minimum value of r = H_2O/TEOS for effective hydrolysis is 2. Variations in r affect the hydrolysis and condensation as well as gelation times[3]. In this study, although the data for different pH regimes at r=4 agree with the structural model as discussed in the last section, overall the data for r=4 and r=10 are not consistent. At pH=1 and r=4, the fast hydrolysis rate and relatively slow condensation rate (section 2.3) should result in a longer decay time than for pH=1,r=10. At p=5, the slower hydrolysis rates relative to condensation should ensure that the water molecules are consumed in the reaction. This, coupled with more colloidal structure predicted for high pH materials, should result in larger values for the decay times. The data in this study does not agree with this model. A more comprehensive study of Eu^{3+} in materials with different r-values was carried out in this laboratory where the materials were densified to 200°C[4]. In that work much better agreement was found between the fluorescence data and the above model. Work is continuing in order to improve the reproducibility of samples with varying r-values.

5.6 Samples Soaked in D_2O

In principle the soaking of samples in D_2O ensures that water and hydroxyl ions in the pores are replaced by D_2O and OD^- ions. Consequently, the decay times should increase. The increased decay times are a result of the reduced non-radiative decay rates (according to equation 5.1), where the deuterium replaces the hydrogen [5]. By comparing the data in tables 5.10 and 5.11 with that in tables 5.7 nad 5.9 for pH 1 it

can be seen that the Eu^{3+} decay times in the presence of D_2O increases by a factor of 2 to 3 for the gel and 200°C samples, and by a smaller amount for the

TABLE 5.10 Lifetime Measurements for Sample Set 2, pH = 1, r = 10, in D_2O.

SAMPLE	METHOD 1 ms(± 0.01)	METHOD 2 ms(± 0.01)	METHOD 3 ms(± 0.01)
Gel	0.26	0.25	0.25
200°C	0.32	0.34	0.34
800°C	2.00	2.21	2.22

TABLE 5.11 Lifetime Measurements for Sample Set 4, pH = 5, r = 10 soaked in D_2O

SAMPLE	METHOD 1 ms(± 0.01)	METHOD 2 ms(± 0.01)	METHOD 3 ms(± 0.01)
Gel	0.25	0.25	0.25
200°C	0.27	0.27	0.27
800°C	1.73	1.77	1.78

800°C sample. For pH=5 these increases are smaller. The data indicates that the hydrogen in the Eu^{3+} environment is only partly replaced by deuterium. Hydroxyl ions in the skeleton will still contribute to the non-radiative decay rate and hydroxyl ions bonded to the pore surface (Silanols) will not necessarily be replaced by OD^- ions.

Thus the increase in the decay time in the presence of D_2O is attributed mainly to the replacement of hydrogen-bonded water in the pores by D_2O. The smaller changes observed at pH=5 are consistent with the lower surface area expected for pH 5=material.

5.7 Chromium as a Sol Gel Probe

Since the discovery of the ruby laser, there has been much interest in Cr^{3+} as an optically active ion in a variety of host materials. In theory chromium should be the best probe of the three studied for this report. Cr^{3+} was used by Bates [6] to establish the ligand field energy of silica glass by comparing the spectra to those of Cr^{3+} in various pH solutions. Bates noted that the Cr^{3+} ion studied must have six oxygen ligands arranged in octahedral symmetry with little departure from regularity as any appreciable random distortion of these groups would show up as an increase in intensity and a broadening of the absorption bands. The electronic transitions of the Cr^{3+} ion are very matrix sensitive as discussed in section 3.9. Broad-band fluorescence from chromium doped glass has been observed and it has been found that the Cr^{3+} transitions are significantly altered by the different ligand fields [7]. In this study, it was found that when the gel was dried above 200°C Cr^{3+} is oxidised to Cr^{6+} as evidenced by its yellow/brown colour. To inhibit this oxidation when samples were being heated for dehydration, arsenic, a strong reducing agent was incorporated in the sol for sample set 5 and 6, a summary of which is given in table 5.12.

TABLE 5.12 Sample sets 5 and 6, Cr^{3+} doped glasses

SAMPLE	r	%Cr	%As	pH
Set 5	20	0.1	1.5	1
Set 6	18.8	0.5	1.5	1

TABLE 5.13 Sample sets 7, 8, 9

SAMPLE	r	%Cr	pH
Set 7	4	0.43	1
set 8	4	0.43	5
Set 9	4	0.43	8

TABLE 5.14 Sample sets 10, 11, 12, and 13

SAMPLE	r	%Cr	pH
Set 10	4	1	1
Set 11	10	1	1
Set 12	4	1	5
Set 13	10	1	5

Samples from each set were cured to 200°C, 500°C and 800°C, respectively. Curing was carried out under hydrogen to eliminate any contact with atmospheric oxygen during densification. This process however did not inhibit oxidation and both the colour and the optical absorption obtained were characteristic of the chromium ion in the +VI oxidation state and no fluorescence was observed from the samples. Nath et al [8] observed that when Cr^{3+} was introduced into melts of silica glass, because of the variable nature of the chromium valency, the ratio of the quantity in the high to that in the low valence state varies with temperature, duration of processing and the nature of the glass.

Chromium doped gels were then produced with processing parameters as summarised in table 5.13. It was decided to concentrate on a study of the sol and gel stage of the process where the Cr^{3+} remained in the trivalent state. The small size of the individual sample pieces hindered absorption measurements as discussed below, but the samples were pale green which demonstrates the presence of Cr^{3+}. No fluorescence was observed when the sample was excited at wavelengths corresponding to Cr^{3+} absorption bands.

A series of more concentrated samples was produced and D_2O replaced H_2O in the production procedure to minimise the concentration of hydroxyl ions. Again no fluorescence was observed. Part of each portion of sample sets 10 to 13 was soaked in D_2O on drying to the gel stage. The fluorescence was believed to be quenched by the hydroxyl groups still present in the matrix, as discussed in section 5.6.

Absorption spectroscopy may be used to examine variations in an ion matrix even if the fluorescence is quenched. A shift towards lower energy of $1540cm^{-1}$ in the absorption peak was observed in the sol to gel transition. This is shown in figure 5.5 and is consistent with previous work on Cr^{3+} in aqueous and glassy environments [6], where the more symmetrical aqueous environment (as in the sol), corresponds to a larger ligand field and hence has a higher energy absorption peak, than the more disordered glassy environment (as in the gel). Thus it is clear that Cr^{3+} has some potential as a probe of the sol-gel environment.

The sharp edges and rough surface of the gel provide many light scattering sites, reducing the S/N of the absorption spectrum. To reduce this, topographic areas must be masked and only a smooth surface exposed to the incident radiation. The glassy samples have small dimensions and are too small to polish. The intensive sample manipulation required posed a severe problem since all acid catalysed glasses tend to fracture and gels of both pH regimes are very brittle. It can be observed that the sensitivity of the d orbital transition to environmental changes offered promising results. Chromium fluorescence was totally quenched in the gel stage by the aqueous matrix. The use of Cr^{3+} as a probe is still being pursued in this laboratory.

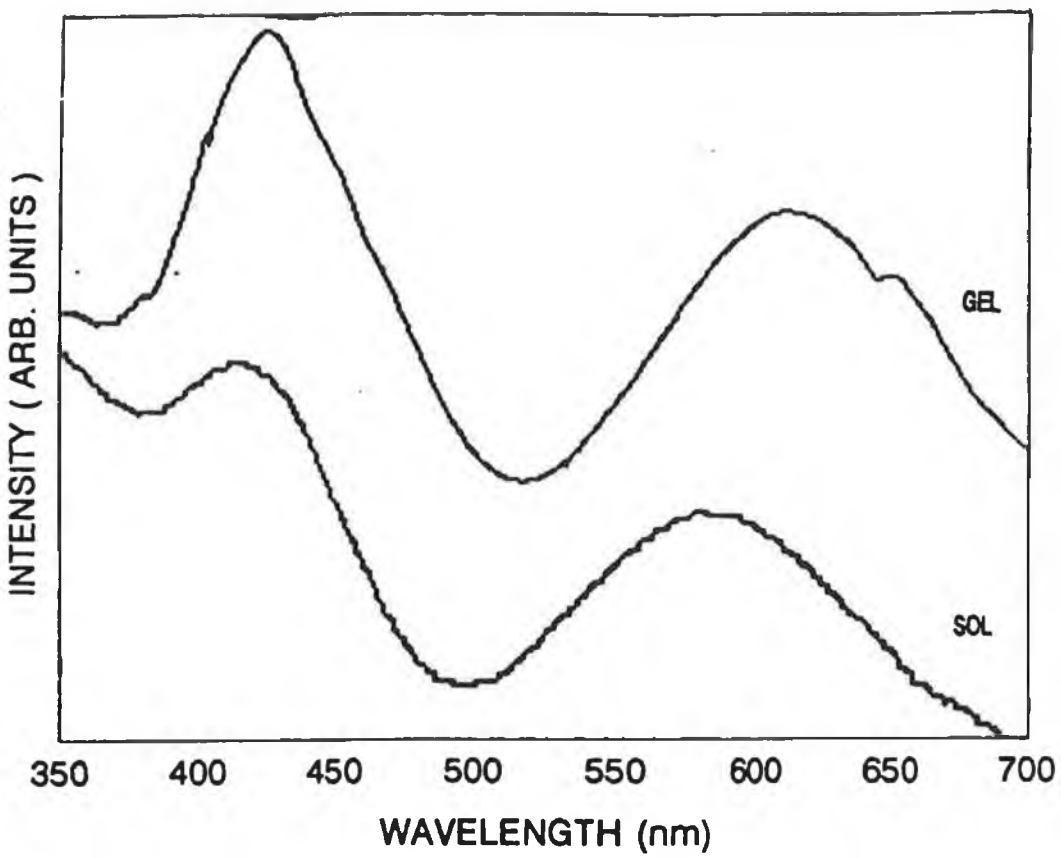

FIGURE 5.5 Absorption Spectra of Cr^{3+} Sol and Gel, pH 1, r = 4

5.8 Conclusion

This study has shown that Eu^{3+} is a sensitive probe of the structural changes in sol-gel glasses. Changes in the optical fluorescence and decay times can be correlated with changes in the Eu^{3+} environment as a function of different processing parameters. By exchanging D_2O for H_2O in the pores it was shown that the short decay time measured was largely due to the non-radiative decay contribution due to the adsorbed water on the pore surface. Soaking experiments in different pH regimes differentiate between the structural models predicted for each pH regime. Finally Cr^{3+} fluorescence

was not observed from sol-gel materials in this study, probably due to quenching by the aqueous environment. It has not been possible so far to maintain the trivalent state at high densification temperatures thereby eliminating water and OH^- ion and achieving the possibility of observing fluorescence. Work is continuing in the laboratory on this problem. However optical absorption can be used as a probe of the material evolution from the sol to gel stage.

CHAPTER 6

URANYL DOPED SOL - GEL MATERIALS

6.1 Introduction

The uranyl ion was doped into silica sol-gel materials synthesised under the same conditions as in the previous chapter and the use of this ion as an optical probe was assessed. The main motivation for studying this ion is the interest in the Eu^{3+} - UO_2^{2+} energy transfer pair which is discussed in chapter 7.

6.2 Optimum Concentration Determination

Samples were made up at 2%, 1% and .5% of UO_2^{2+} atom percent of Silica. Initially a series of samples was prepared at various uranyl concentrations to determine the smallest concentration suitable for adequate signal, while simultaneously keeping the possibility of clustering and concentration quenching to a minimum. The .5% sample gave no signal in the sol while the 2% sample fluoresced. The 1% sample also fluoresced and was more likely to be homogeneously distributed than the larger concentration. A uranyl concentration of 1% was decided upon.

6.3 Samples Produced for Analysis

Sample sets 14 to 17 contained 1% UO_2^{2+}, the r values and pH of sol solution are given in table 6.1.

TABLE 6.1 UO_2^{2+} samples produced for analysis

SAMPLE	r	pH
Set 14	4	1
Set 15	10	1
Set 16	4	5
Set 17	10	5

A quantity of sets 15 and 17 was soaked in D_2O for 1 week. A quantity of sets 14 and 16 were soaked in 1% $Eu(NO_3)_3$ for 1 week. Results obtained with these samples will be discussed in Chapter 7. A quantity of set 14 gel was heated to 1400°C.

6.4 Spectral Variation as a Function of Temperature

The fluorescence of the UO_2^{2+} ion is due to transitions from the first excited state to the vibrational levels of the system in the ground state. These vibronic transitions arise from symmetric and anti-symmetric vibrations of the U-O bond as discussed in section 3.1. Figures 6.1 to 6.4 display the spectral variation for each of the samples. Taking sample set 15 (pH = 1, r = 4) as representative of the spectral trends with temperature, it can be noted from fig. 6.1 that the vibrational levels in the sol stage are not resolved. The spectrum consists of a smooth single peaked band. The existence of alternative sites in the gel stage manifests itself in sharp peaks (similar to that of UO_2^{2+} in phosphate glass[1]) in the range 460nm - 490nm. These peaks start to disappear as the loose cage structure starts to dry out at 200°C. The gel, 200°C and 800°C spectra consist primarily of three broad bands whose overall structure does not change with temperature. The main feature is the small red shift observed for the 800°C spectrum with respect to the gel and 200°C spectrum. This is consistent with previous work [1] on uranyl-doped phosphate glasses where a red shift in fluorescence was observed in going from a weakly bonded aqueous environment to a more strongly bonded glassy environment.

The separations between the fluorescence peaks correspond to the vibrational energy level separations of the U-O bond. This energy difference should vary with U-O bond strength. For example, these intervals in uranyl doped soda-lime glass are of the order of 750cm^{-1}[2] while in aqueous uranyl solution the separation is about 850cm^{-1}[3]. The spectra in figure 6.1 show an average energy interval of about 700cm^{-1} for both gel and glassy material. This suggests that either the associated ligand field is changing only slightly or that the relative vibrational transitions of the molecular probe are insensitive to changes in the

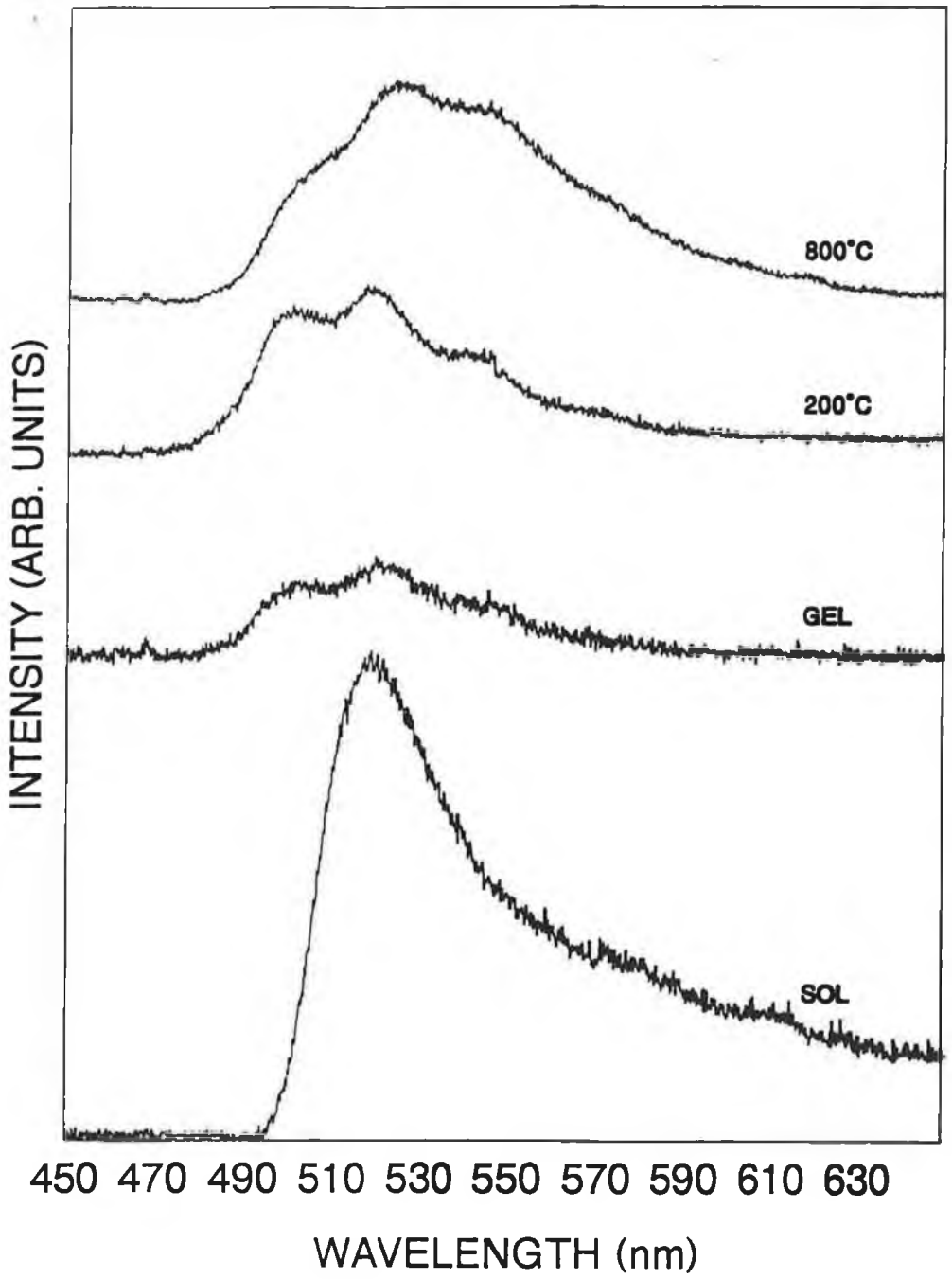

FIGURE 6.1 Fluorescence Spectra of Sample Set 14, pH 1, r = 4

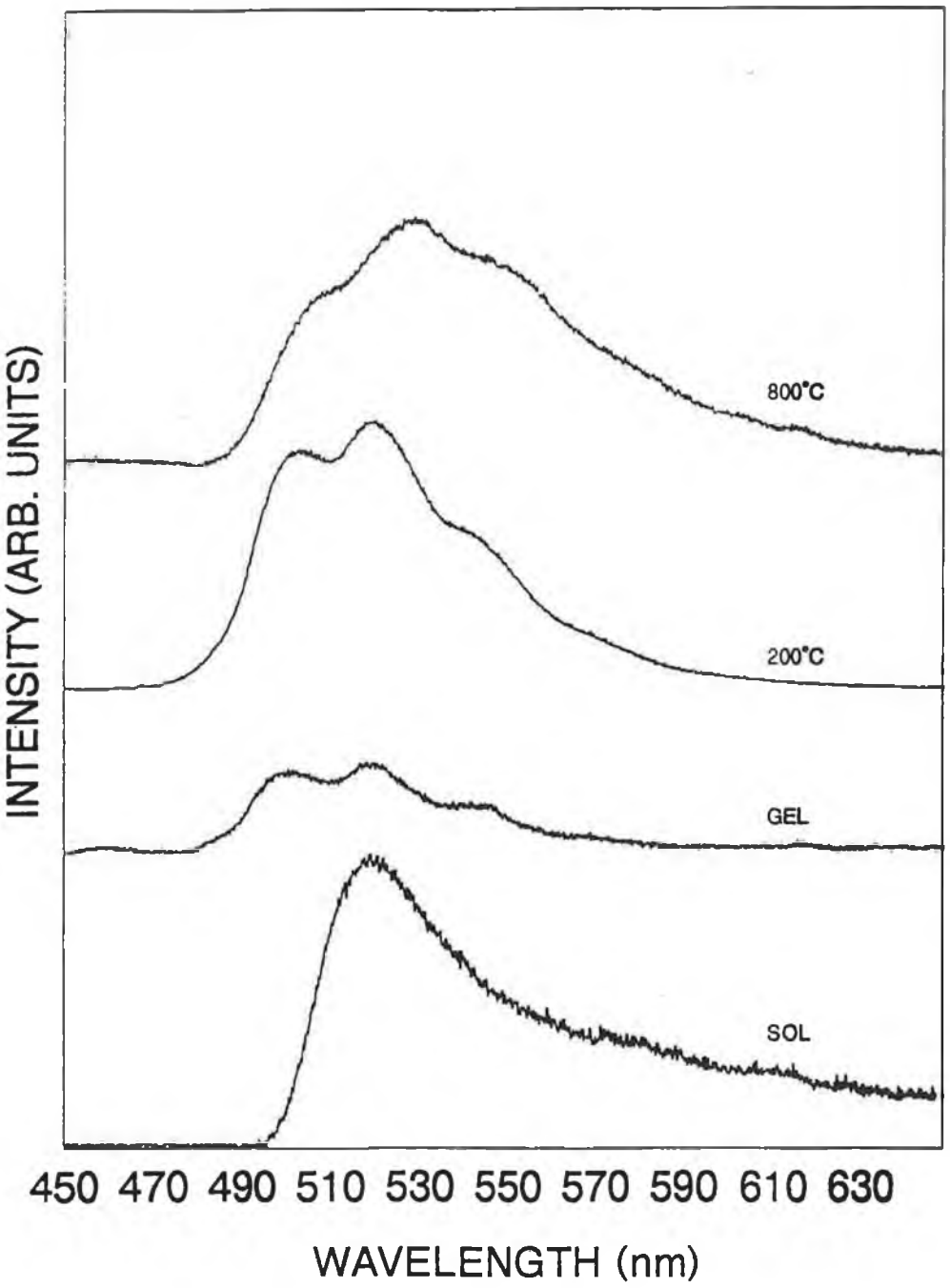

FIGURE 6.2 Fluorescence Spectra of Sample Set 15, pH 1, r = 10

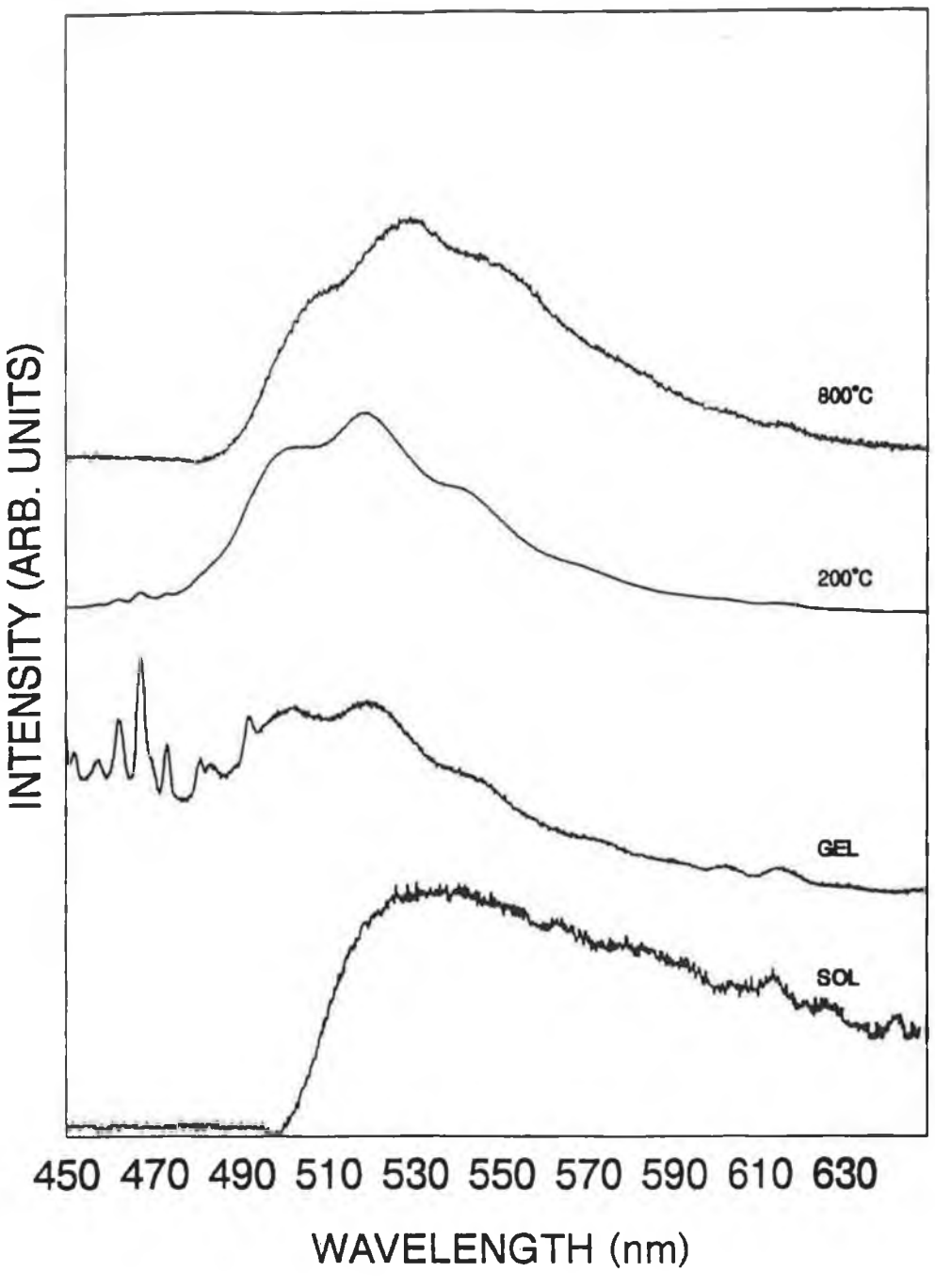

FIGURE 6.3 Fluorescence Spectra of Sample Set 16, pH 5, r = 4

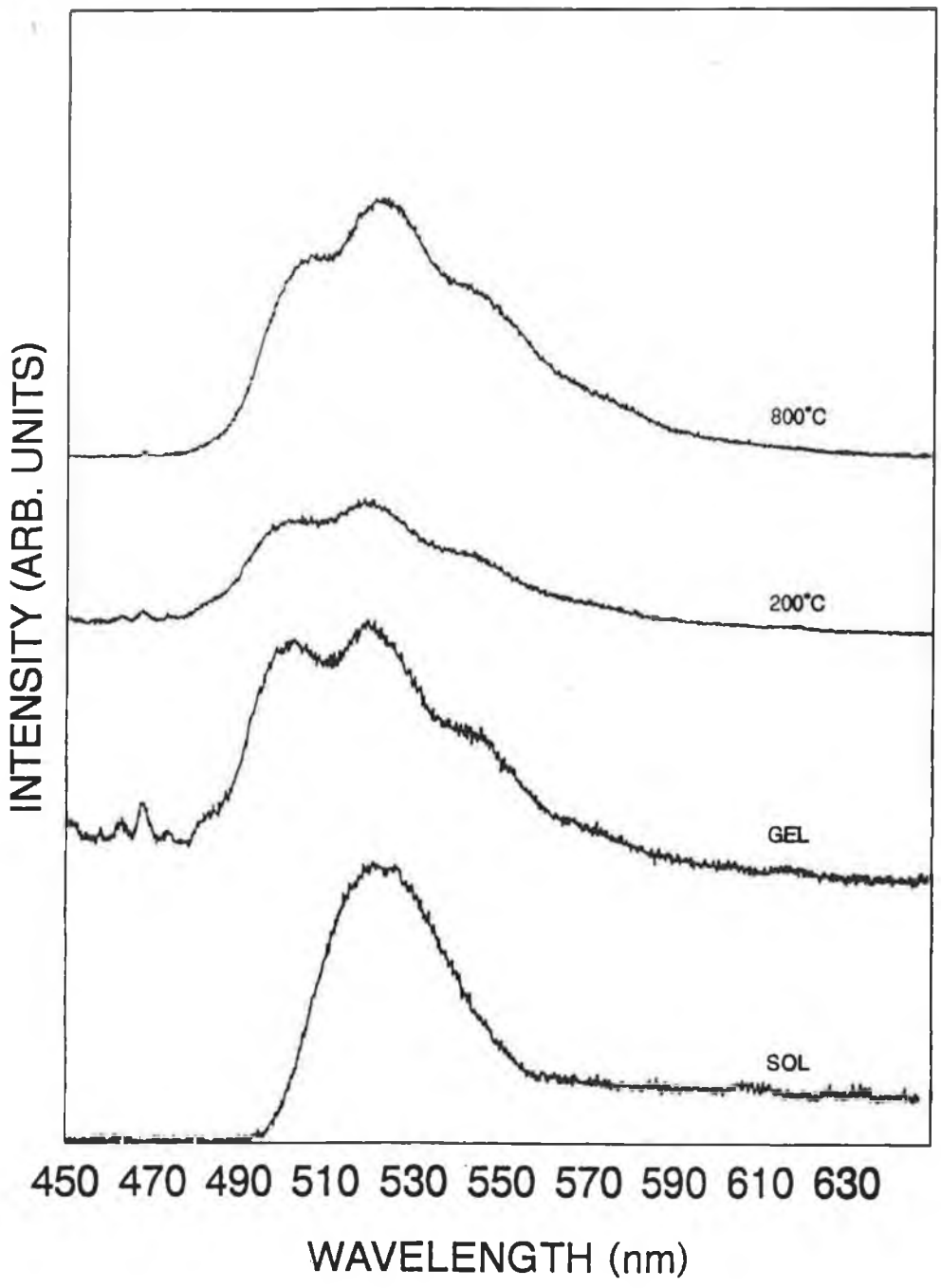

FIGURE 6.4 fluorescence Spectra of Sample Set 17, pH 5, r = 10

TABLE 6.2 Lifetime Values for Sample Set 14, pH = 1, r = 4

SAMPLE	METHOD 1 ms(± 0.01)	METHOD 2 ms(± 0.01)	METHOD 3 ms(± 0.01)
Sol	0.11	0.12	0.12
Gel	0.10	0.11	0.12
200°C	0.12	0.14	0.14
800°	0.16	0.18	0.18
1400°C	0.26	0.27	0.27

TABLE 6.3 Lifetime Values for Sample Set 15, pH = 1, r = 10

SAMPLE	METHOD 1 ms(± 0.01)	METHOD 2 ms(± 0.01)	METHOD 3 ms(± 0.01)
Sol	0.11	0.11	0.12
Gel	0.10	0.11	0.12
200°C	0.13	0.14	0.14
800°C	0.16	0.17	0.17

matrix. From observations made in Chapter 5 and from lifetime variations with temperature in tables 6.2 to 6.5 it is obvious that there are environmental changes in each stage of the process. Hence it is concluded that the room temperature uranyl ion vibrational transitions are insensitive to changes in the matrix environment. The lifetime data displayed in Tables 6.2 to 6.5 display the same trends observed in europium ion spectroscopy. The lifetime decreases from the sol to the gel, indicating a larger water presence. The value then proceeds to increase on drying to a maximum

TABLE 6.4 Lifetime Values of Sample Set 16, pH = 5, r = 4

SAMPLE	METHOD 1 ms(± 0.01)	METHOD 2 ms(± 0.01)	METHOD 3 ms(± 0.01)
Sol	0.10	0.11	0.11
Gel	0.10	0.10	0.10
200°C	0.12	0.12	0.13
800°C	0.15	0.15	0.16

TABLE 6.5 Lifetime Values of Sample Set 17, pH = 5, r = 10

SAMPLE	METHOD 1 ms(± 0.01)	METHOD 2 ms(± 0.01)	METHOD 3 ms(± 0.01)
Sol	0.10	0.11	0.11
Gel	0.09	0.10	0.10
200°C	0.13	0.14	0.14
800°C	0.16	0.16	0.17

of 0.26ms at 1400°C. The lifetime of Uranyl ion in conventional phosphate glass is 0.37 ms[1] so there is some evidence of the existence of fluorescence quenchers at 1400°C in the sol-gel glasses. This was not observed in Eu^{3+}-doped glass indicating that UO_2^{2+} in some way hinders pore closure and final hydroxyl group removal. This effect will be discussed further in chapter 7.

6.5 Spectral Variation with pH

UO_2^{2+} has been found to be pH sensitive in aqueous solutions[3]. It is a strong oxidising agent and oxidises water liberating protons. Sols produced by water of pH=1 had a final pH of 0.6, while sols produced by water of pH=5 had a final pH of 2.5. This decrease in pH indicates a proton liberating reaction.

It appears, however, that UO_2^{2+} is not pH sensitive in sol-gel silica. The sol spectra are similar for each pH and the lifetime variation is within the error bars from acidic to basic samples. The spectra and lifetime values of the gel, 200°C and 800°C do not vary significantly with pH either.

This insensitivity to pH may be partly due to the fact that it is the initial pH of the water for hydrolysis in the sols that determines the structural evolution pattern. In the sol the overall pH can adjust itself due to the hydrolysis and condensation reactions, for example a small pH variation was observed in the Eu^{3+} doped sols. This redox reaction in the sol stage brings the 'base' samples near to the isoelectric point of silica thus minimising the difference between the two pH samples. Hence it is the oxidising nature of the ion that makes it unsuitable as a probe for sol-gel materials. Its reactivity in the sol appears to cause a complex pH behaviour whereby the overall pH is altered drastically from initial conditions.

6.6 Spectral Variations as a Function of r

As previously stated, spectral variation is observed on dehydration to 800°C . The uranyl ion seems insensitive to variations induced by altering the other process parameters, such as pH and water/TEOS ratio. There is no variation observed in either the spectra or the lifetime values as a function of the r ratio. In acid-catalysed media the higher r ratio encourages hydrolysis while inhibiting condensation and a highly ramified chain structure results. The π electron cloud of the uranyl ion may inhibit close association with the Si-O skeleton and as a result, alterations to this structure may not alter the fluorescence of the ion. Base-catalysed samples are insensitive to variations in r also.

6.7 Samples Quenched in D_2O

As stated in section 5.6 soaking a sample in D_2O should ensure that water and hydroxyl ions in the pores are replaced by D_2O and OD^- ions whereby the decay times should increase but it was found that only partial substitution occurs.

Lifetime data for samples soaked in D_2O are displayed in Tables 6.6 and 6.7. According to Eqn. 5 an increase in decay time indicates a lower non-radiative decay rate in the presence of deuterium. There is an increase in the lifetime values

TABLE 6.6 Lifetime Values of Acid Catalysed Gel in D_2O

SAMPLE	METHOD 1 ms(± 0.01)	METHOD 2 ms(± 0.01)	METHOD 3 ms(± 0.01)
Gel	0.26	0.25	0.25
200°C	0.20	0.22	0.23
800°C	0.21	0.22	0.23

TABLE 6.7 Lifetime Values of Base Catalysed Gel in D_2O

SAMPLE	METHOD 1 ms(± 0.01)	METHOD 2 ms(± 0.01)	METHOD 3 ms(± 0.01)
Gel	0.24	0.25	0.25
200°C	0.17	0.17	0.18
800°C	0.18	0.18	0.19

compared to those in Tables 6.2 and 6.4. The pH=1 samples show a larger increase than the pH=5, due to the larger surface area expected from samples produced at pH < 2[4], which is consistent with the Eu^{3+} data in section 5.6. This larger surface area would allow greater D_2O mobility and a greater D - H exchange. The lifetime values are still less than those obtained for the fully dehydrated 1400°C sample. Possible reasons for this are that the hydrogen ions on the surface were only partially replaced by deuterium as in the case of europium-doped silica gels; hydroxyl ions in the skeleton will contribute to the non radiative decay as previously stated in Section 5.6.

6.8 Comparison of Eu^{3+} and UO_2^{2+} as Structural Probes

Eu^{3+} proves to be a more sensitive probe at room temperature. It has a larger quantum yield and three resolved transitions. The characteristics of each of the three transitions

can be exploited to further probe the matrix of the ion. The uranyl ion has two π bonds forming an electrostatic field perpendicular to the plane of the molecule. The electrostatic repulsion arising from this may reduce its association with the Si-O network. Europium on the other hand is strongly associated to the oxygen lone pairs and to non-bridging oxygens. Any change in this network would, therefore, be observed in the europium ion luminescence. The positive change in the uranyl ion does bond in the plane of the molecule. Any variation outside this plane would not alter the energy of state of the uranyl ion. Indeed the energetics of the various vibrational modes of the linear molecule do not change with respect to each other throughout the whole process of dehydration. The uranyl ion is also a strong oxidising agent which alters the sol pH dramatically. The excitation of UO_2^{2+} ion can be quenched by water via a hydrogen abstraction reaction

$$UO_2^{2+} + H_2O \rightleftharpoons UO_2OH^- + H^+ \qquad (6.2)$$

This type of quenching also alters the pH, both of the sol and the matrix water remaining in the higher temperature materials. Hence it is difficult to interpret pH data in terms of structural changes. In general the UO_2^{2+} optical data confirms results obtained for Eu^{3+} in chapter 5.

6.9 Summary

This chapter discussed the fluorescence and lifetime data for uranyl doped silica samples. The UO_2^{2+} ion was found to alter drastically the sol pH and overall is a less sensitive probe than Eu^{3+} at room temperature, partly due to its chemical interactions with the sol and partly due to its insensitivity to alterations in the ligand field.

CHAPTER 7

EUROPIUM AND URANYL CO-DOPED MATERIALS AND ENERGY TRANSFER EFFECTS

7.1 Introduction

Sol-gel silica was codoped with Eu^{3+} and UO_2^{2+} in order to investigate the occurrence of energy transfer, and to exploit this energy transfer to determine pore morphology.

7.2 Energy Transfer in Solids

In materials which have been doped with large concentrations of optically active species, transfer of energy can occur between similar and different species[1]. In general the criteria for energy transfer to occur are (i) that the ions are in close proximity to each other and (ii) that the absorption of the acceptor ion overlaps with the fluorescence of the donor ion. The donor - acceptor energy transfer route is an alternative pathway for donor deexcitation and it competes with radiative deexcitation of the donor to the ground state. The mechanisms for energy transfer may be an exchange interaction (if the wave functions overlap) or an electric or magnetic multipolar interaction[1]. A decrease in fluorescence intensity of the donor ion from a singly-doped sample to a co-doped sample is evidence of possible energy transfer in that the donor fluorescence is quenched. This should be accompanied by a decrease in donor lifetime as the energy transfer process provides an alternative pathway for donor deexcitation. An examination of the excitation spectrum of the acceptor ion also verifies the occurrence of energy transfer as the excitation spectrum should contain both acceptor and donor bands. The transfer efficiency between donor and acceptor ions, η_{da}, is given by

$$\eta_{da} = 1 - \frac{\eta_d}{\eta_d^0} = 1 - \frac{\tau_d}{\tau_d^0} \qquad (7.1)$$

where η_d^0 and τ_d^0 are the quantum efficiency and lifetime of the donor in the absence

of the acceptor and η_d and τ_d are the same in the presence of the acceptor[1]. It is assumed that fluorescence from the donor is only observed when there is no acceptor within a critical volume for quenching. The efficiency for energy transfer therefore can then be given as

$$\eta_{da} = 1 - e^{-VC_a} \qquad (7.2)$$

where C_a is the number of acceptor ions per unit volume, and V is the quenching volume, given by

$$V = (4/3)\,\pi\, R_{da}^{3} \qquad (7.3)$$

where R_{da} is the maximum inter-ion radius allowable for energy transfer to occur between dopant ions[2].

In this study sol-gel silica is doped with UO_2^{2+} and Eu^{3+} as the donor-acceptor pair. This system has been studied in conventional glasses where energy transfer was observed using ion concentrations similar to those used here[3]. This ion pair is a suitable candidate for energy transfer studies as the uranyl fluorescence overlaps the Eu^{3+} absorption bands. Initially a study was made of UO_2^{2+}-Eu^{3+} co-doped materials to verify that energy transfer occurs in these sol-gel materials. Subsequently, samples were synthesised where uranyl-doped materials, densified to various temperatures, were soaked in a europium nitrate solution, equivalent to 2% doping and then dried. It was hoped that the energy transfer effects observed in these materials would give some structural information, in particular on the porosity.

7.3 Samples Prepared for Energy Transfer Studies

The r and pH values used in the production of sample sets 18 to 21 are given in table 7.1.

Samples sets 18 and 19 (hereafter referred to as co-doped) contained 1% UO_2^{2+} and 2% Eu^{3+}. Samples 20 and 21 (referred to as post-doped) contained 1% UO_2^{2+} and were soaked in a 2% europium nitrate solution.

TABLE 7.1 Sample Sets 18, 19, 20 and 21

SAMPLE	r	pH
Set 18	4	1
Set 19	4	5
Set 20	4	1
Set 21	4	5

7.4 Fluorescence Spectra and Decay Times of Co-Doped Samples

Sample sets 18 and 19 were synthesised to examine whether or not energy transfer occurs between UO_2^{2+} and Eu^{3+} in sol-gel silica. An excitation spectrum of the $^5D_0$-$^7F_2$ fluorescent peak for Eu^{3+} in sample 18 is shown in figure 7.1.

Peaks were observed at 398nm, 421nm, 462nm, and 527nm. The 398nm and 462nm peaks are characteristic of Eu^{3+} but the 421nm and 527nm peaks are UO_2^{2+} absorption bands, confirming that UO_2^{2+} pumps Eu^{3+} when the ions are codoped in the materials. Tables 7.2 to 7.5 display the lifetime values of Eu^{3+} and UO_2^{2+}. It is clear that the uranyl lifetimes have decreased relative to singly doped uranyl (tables 6.2 to 6.5) confirming that energy transfer is occurring. There is a larger decrease for the more densified samples indicating that the amount of hydration of the material directly influences the energy transfer between ions. In principle the Eu^{3+} lifetimes should not change. However, as can be seen from tables 7.2 and 7.4, these lifetimes are decreased relative to those of singly doped Eu^{3+} (see tables 5.6 to 5.9) particularly at higher densification temperatures. This decrease is attributed to backtransfer effects. Back transfer has been observed in other energy transfer systems where the acceptor ion relaxes via the faster relaxing donor ion [2] Tables 7.6 and 7.7 display the transfer efficiencies calculated from the decay times according to equation 7.1. For both pH regimes, the efficiency increases with densification temperature, due to the removal of hydroxyl ions and the increase in the density of the material (smaller inter-ion spacing). The efficiencies are larger for pH = 1 materials which is consistent with the finer texture of these low pH sol-gel materials.

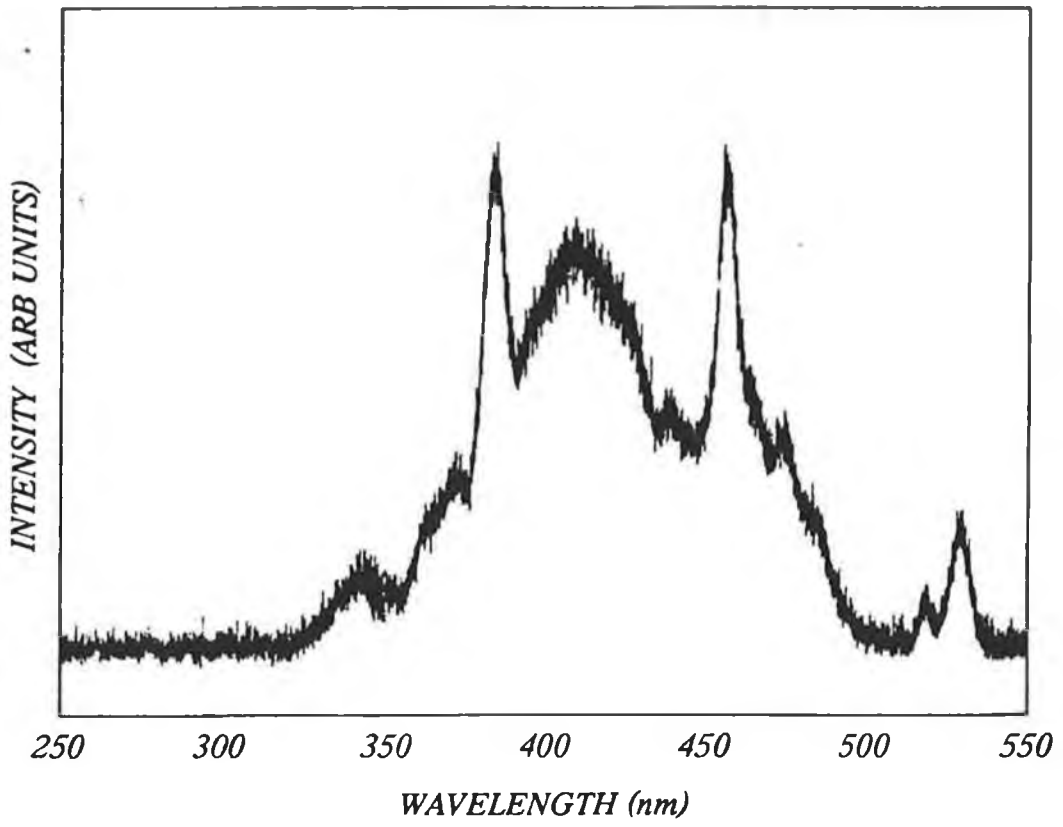

FIGURE 7.1 Eu^{3+} Excitation

In these structures Eu^{3+} and uranyl ions are likely to be in closer proximity to each other than the more colloidal base-catalysed materials.

Table 7.2 Lifetime values of Eu^{3+} in sample set 18, pH = 1, r = 4

SAMPLE	METHOD 1 ms(±.01)	METHOD 2 ms(±.01)	METHOD 3 ms(±.01)
Gel	0.13	0.13	0.14
200°C	0.23	0.24	0.24
800°C	0.67	0.69	0.68
1400°C	0.69	0.69	0.69

Table 7.3 Lifetime values of UO_2^{2+} in sample set 18, pH = 1, r = 4

SAMPLE	METHOD 1 ms(±.01)	METHOD 2 ms(±.01)	METHOD 3 ms(±.01)
Gel	0.10	0.10	0.10
200°C	0.10	0.11	0.11
800°C	0.08	0.08	0.08
1400°C	0.02	0.03	0.03

Table 7.4 Lifetime values of Eu^{3+} in sample set 19, pH = 5, r = 4

SAMPLE	METHOD 1 ms(±.01)	METHOD 2 ms(±.01)	METHOD 3 ms(±.01)
Gel	0.17	0.17	0.18
200°C	0.32	0.33	0.33
800°C	0.68	0.69	0.70
1400°C	0.69	0.69	0.69

Table 7.5 Lifetime values of UO_2^{2+} in sample set 19, pH = 5, r = 4

SAMPLE	METHOD 1 ms(±.01)	METHOD 2 ms(±.01)	METHOD 3 ms(±.01)
Gel	0.10	0.10	0.10
200°C	0.10	0.10	0.10
800°C	0.09	0.09	0.09
1400°C	0.03	0.04	0.04

TABLE 7.6 Energy Transfer Efficiency of sample set 18, pH = 1, r = 4

SAMPLE	η (+/-.02)
Gel	0.09
200°C	0.17
800°C	0.43
1400°C	0.92

TABLE 7.7 Energy Transfer Efficiency of Sample Set 19, pH = 5, r = 4

SAMPLE	η (+/-.02)
Gel	0.02
200°C	0.19
800°C	0.30

Figures 7.2 and 7.3 show the fluorescence spectra for these co-doped materials. From the spectra it is difficult to quantify the amount of UO_2^{2+} quenching present. From the lifetime data, it is obvious that the presence of back transfer effects complicates the situation in sofar as the Eu^{3+} fluorescence is probably also quenched. Hence in these materials the most convincing evidence of the occurrence of energy transfer comes from the excitation spectra and lifetime data

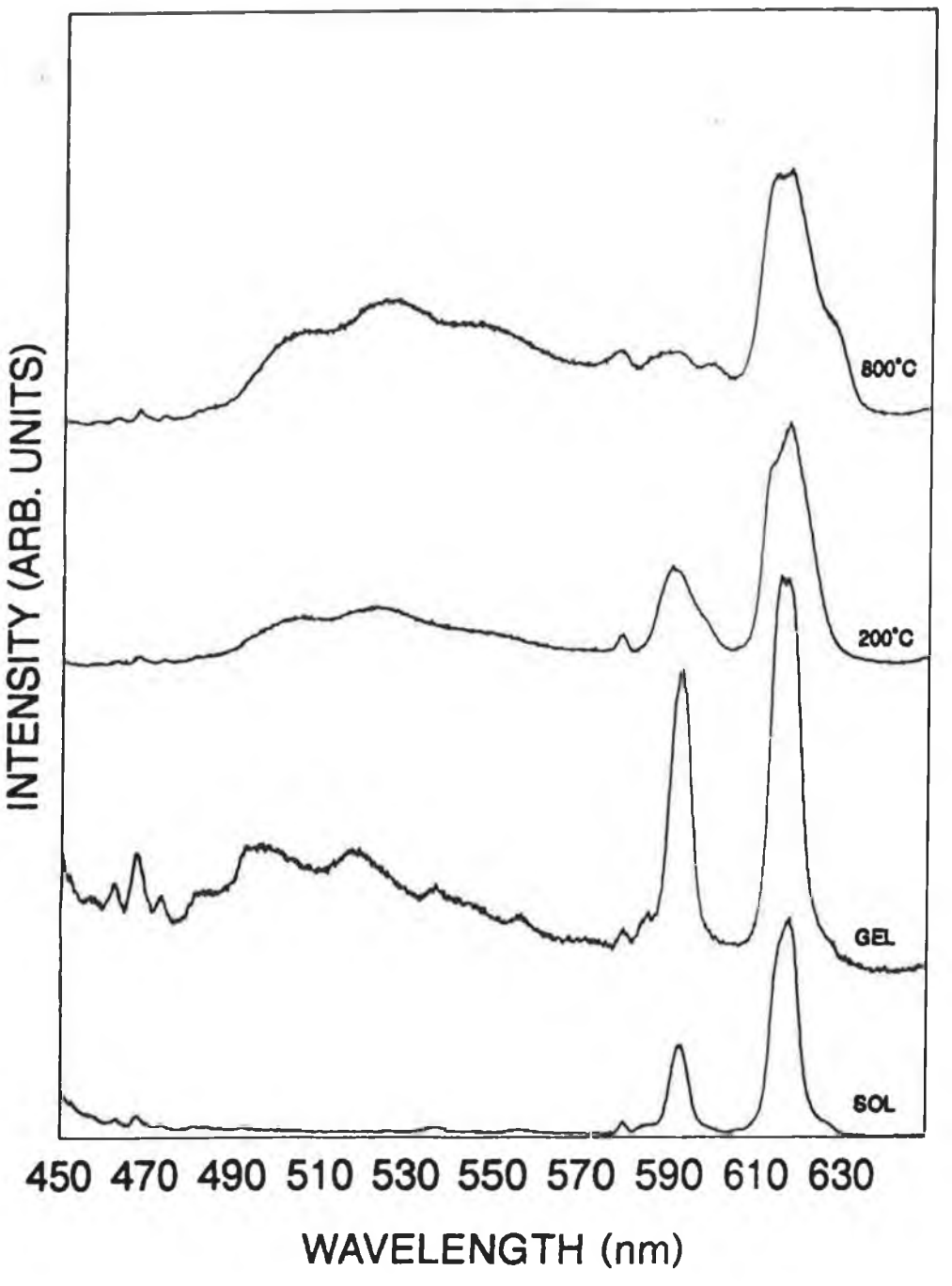

FIGURE 7.2 Fluorescence Spectra of Sample Set 18

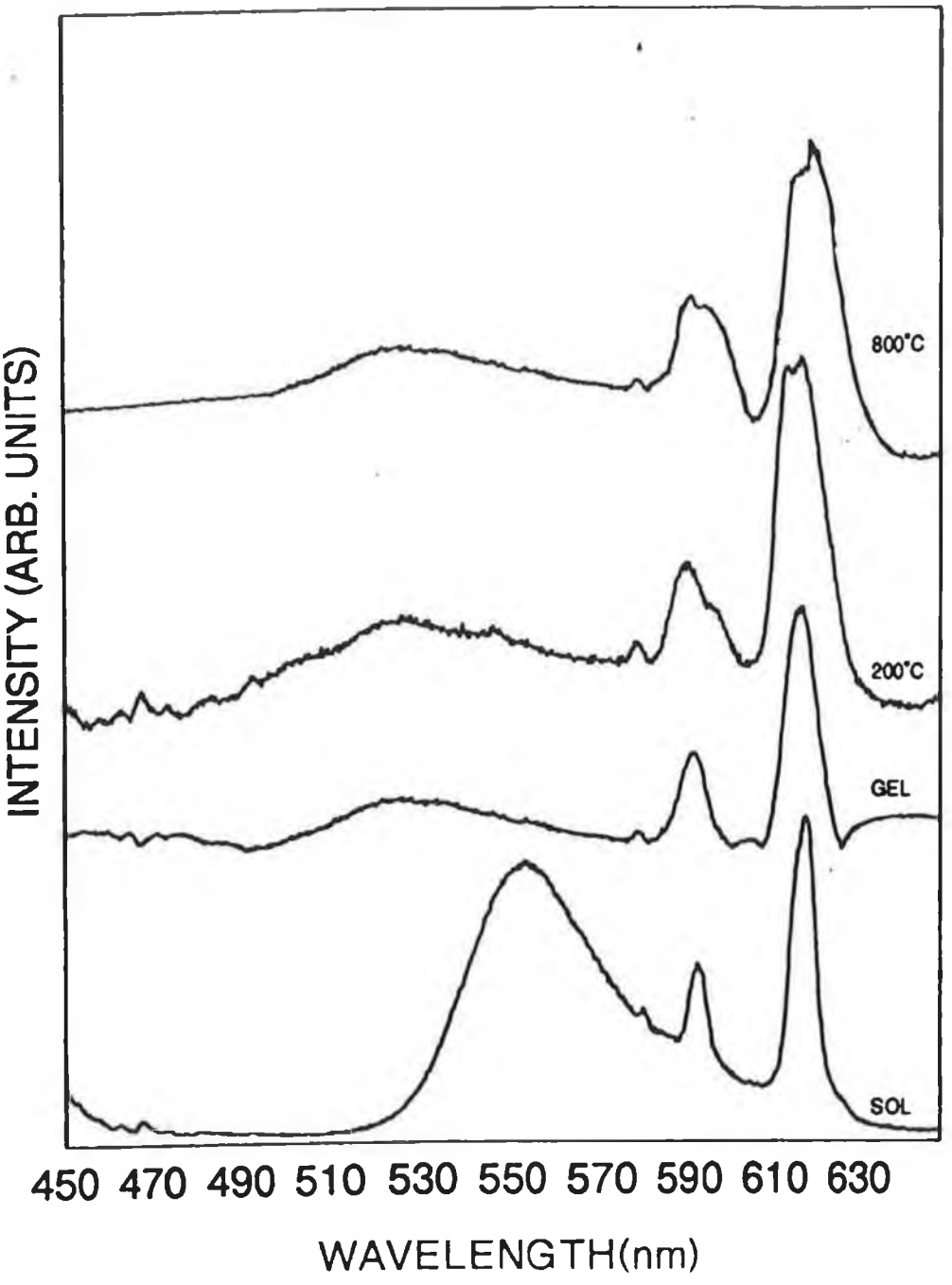

FIGURE 7.3 Fluorescence Spectra of Sample Set 19

7.4 Samples Soaked in $Eu(NO_3)_3$ (post-doped)

Samples were soaked in $Eu(NO_3)_3$ to investigate energy transfer effects between uranyl ions in the skeleton and Eu^{3+} in the pores thus probing the pore morphology. The samples were synthesised under conditions identical to those of sample sets 5 and 7 as discussed in chapter 6.The samples are described in table 7.1. The Eu^{3+} was incorporated by soaking each sample in a 2% $Eu(NO_3)_3$ solution for one week and subsequently drying the sample. The gels are dried at 73°C for four days. The 200°C and 800°C samples are dried at 150°C for 24 hours. Tables 7.8 to 7.11 show the lifetime values for Eu^{3+} and UO_2^{2+} for the above samples.

TABLE 7.8 Lifetime Values of Eu^{3+} in Sample Set 20, pH = 1, r = 4

SAMPLE	METHOD 1 ms(+/.01)	METHOD 2 ms(+/-.01)	METHOD 3 ms(+/-.01)
Gel	0.09	0.09	0.10
200°C	0.11	0.12	0.12
800°C	0.14	0.15	0.17

TABLE 7.9 Lifetime Values of UO_2^{2+} in Sample Set 20, pH = 1, r = 4

SAMPLE	METHOD 1 ms(+/-.01)	METHOD 2 ms(+/-.01)	METHOD 3 ms(+/-.01)
Gel	0.10	0.11	0.11
200°C	0.10	0.10	0.10
800°C	0.11	0.12	0.12

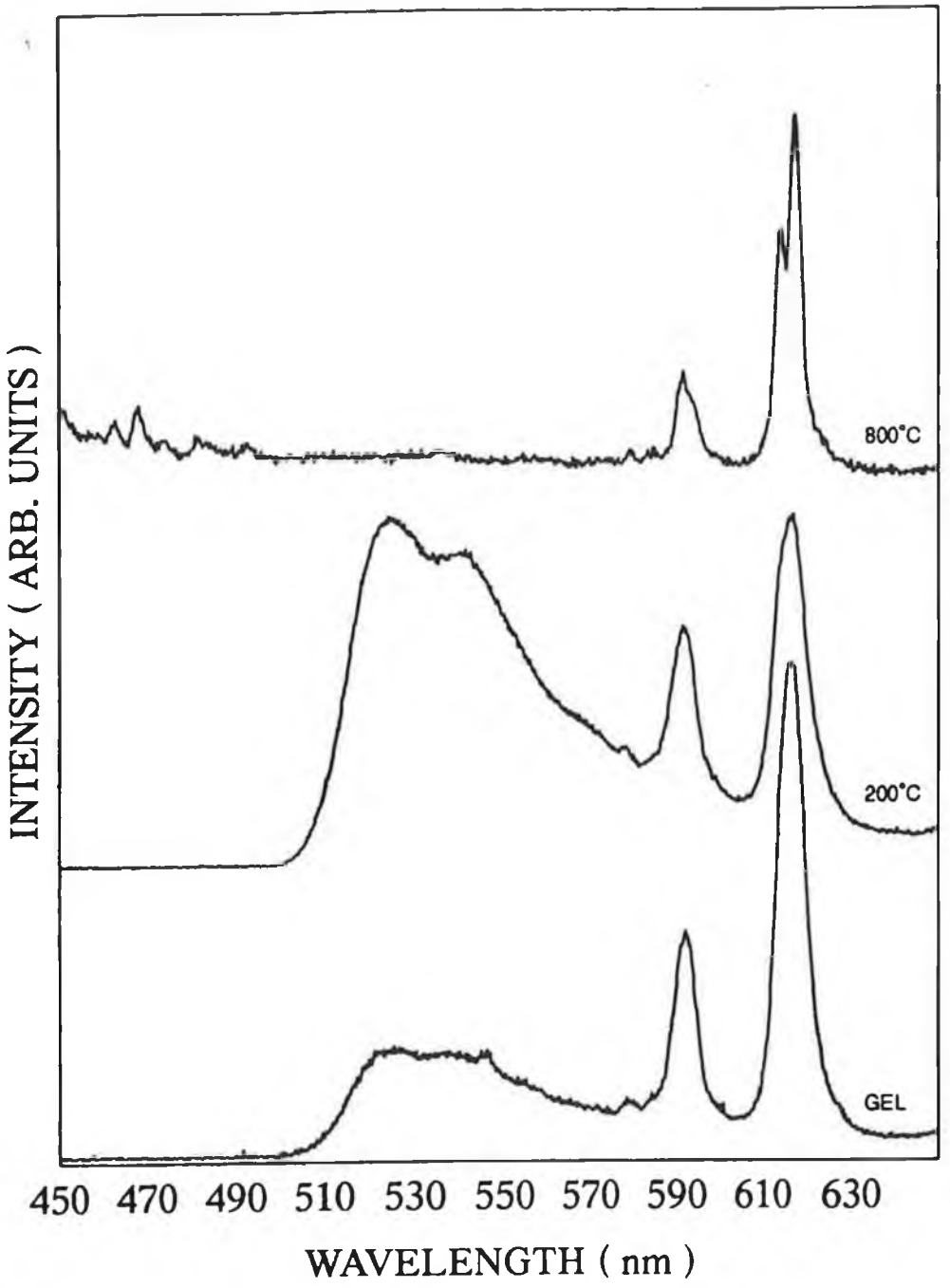

FIGURE 7.4 Fluorescence Spectra of Sample Set 20

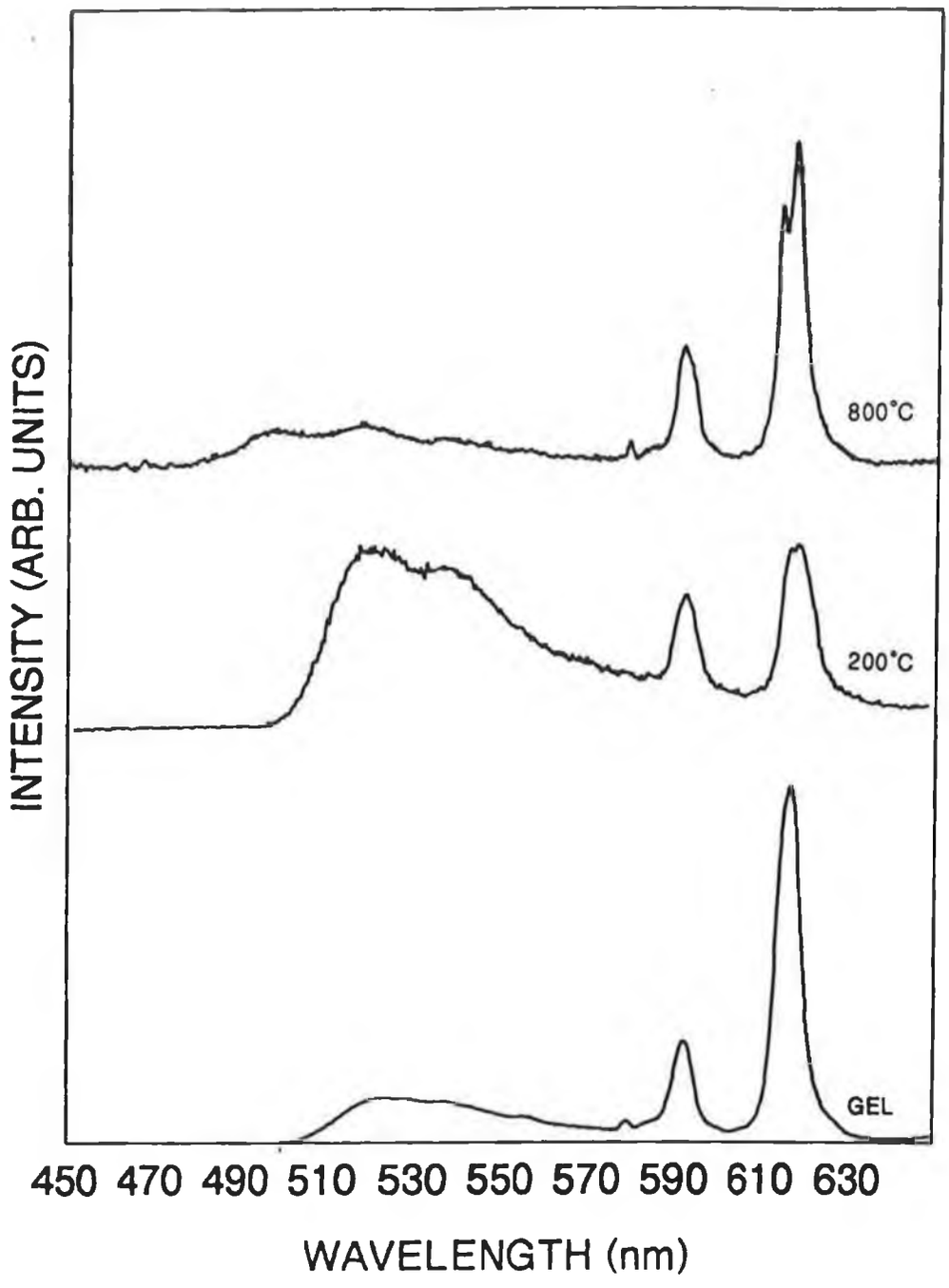

FIGURE 7.5 Fluorescence Spectra of Sample Set 21

TABLE 7.10 Lifetime Values of Eu^{3+} in Sample Set 21, pH = 5, r = 4

SAMPLE	METHOD 1 ms(+/-.01)	METHOD 2 ms(+/-.01)	METHOD 3 ms(+/-.01)
Gel	0.11	0.12	0.13
200°C	0.14	0.15	0.15
800°c	0.12	0/13	0.13

TABLE 7.11 Lifetime Values of UO_2^{2+} in Sample Set 21, pH = 5, r = 4

SAMPLE	METHOD 1 ms(+/-.01)	METHOD 2 ms(+/-.01)	METHOD 3 ms(+/-.01)
Gel	0.10	0.10	0.10
200°C	0.11	0.11	0.12
800°C	0.12	0.13	0.14

TABLE 7.12 Energy Transfer Efficiency of Sample Set 20, pH = 1, r = 4

SAMPLE	η (+/-.02)
Gel	0.04
200°C	0.20
800°C	0.30

TABLE 7.13 Energy Transfer Efficiency of Sample Set 21, pH = 5, r = 4

SAMPLE	η (+/-.02)
Gel	0.02
200°C	0.08
800°C	0.22

The Eu^{3+} lifetimes (tables 7.8 and 7.10) are synonymous with those of the ions soaked in water as discussed in chapter 5. This is consistent with the accepted model for the pores whereby a layer of hydroxyl ions is present on the pore surface even after drying at relatively high temperatures. Tables 7.9 and 7.11 show that the UO_2^{2+} lifetimes decrease in value in the presence of Eu^{3+} in the nearby pores, as was the case for the co-doped samples discussed in the previous section. Thus energy transfer occurs between UO_2^{2+} in the skeleton and Eu^{3+} in the pores. The transfer efficiencies in tables 7.12 and 7.13 show similar trends as for the co-doped samples in that the efficiency increases with densification temperature and is greatest for low pH materials. Since Eu^{3+} is now in the pores and not in the skeleton, the higher efficiency for low pH indicated that the UO_2^{+} inter-ion distance is on average smaller for low pH materials. This conclusion is consistent with the finer pore texture and larger surface area found for acid-catalysed sol-gel silica compared to base-catalysed materials[4]. Hence the larger pore surface area enables more Eu^{3+} ions to adsorb onto the pore surface and to absorb energy from nearby UO_2^{2+} ions. For the base-catalysed materials on the other hand, larger pores and smaller surface area reduces the number of Eu^{3+} ions which come in close proximity to the UO_2^{2+} ions in the more colloidal skeletal structure. The fluorescence spectra in figures 7.4 and 7.5 confirm the presence of hydroxyl ions in the vicinity of the Eu^{3+} ion in that the Eu^{3+} transitions are sharp and exhibit very little structure. These spectra again verify the presence of a layer of hydroxyl ions on the pore surface even after drying at elevated temperatures. Quantitative quenching effects cannot be deduced from these spectra as

Eu^{3+}fluorescence is quenched in the presence of hydroxyl ions, as is the case for the co-doped samples discussed in the previous section, the most convincing evident of energy transfer comes from the lifetime data. From this preliminary study it appears that energy transfer studies can give structural information about these porous materials.

7.5 Summary

Energy transfer between UO_2^{2+} and Eu^{3+} can be observed in sol-gel materials. The efficiency of this energy transfer increases with increasing densification temperature. Energy transfer efficiency is greater for the acid-catalysed gels than for the base-catalysed materials. The colloidal nature of the base-catalysed material is more likely to shield the ion from acceptors than the ramified acid-catalysed chain structure. The Eu^{3+} lifetime in the codoped material is significantly shorter than the singly-doped material, probably due to back transfer of the pumping energy.

CHAPTER 8

CONCLUSIONS AND PROPOSALS FOR FUTURE WORK

It is clear from chapter 5 that the Eu^{3+} ion is a useful and effective probe in the structural analysis of silica gels. Structural variations with temperature, pH, and r ratio reflected in the associated variations of the Eu^{3+} ion spectra agree with the proposed models[1]. Chromium was found to be an ineffective probe of the sol-gel process since its luminescence is quenched in the gel and heat treatment for dehydration alters its oxidation state.

From chapter 6 it is concluded that UO_2^{2+} is a less effective probe than Eu^{3+}. However the spectra do verify some results discussed in chapter 5. The existence of surface silanols on the pores, hydroxyl groups within the closer cage structure, and the strengthening of the ligand field on dehydration to 800°C was verified by the uranyl ion spectroscopy.

Chapter 7 shows that UO_2^{2+} pumps Eu^{3+} when the two ions are codoped in silica gels. The efficiency of this energy transfer increases with dehydration. Samples soaked in $Eu(NO_3)_3$ also exhibit energy transfer and these results give some structural information.

Chromium may be a useful probe of thin films dried to the gel stage, as absorption would be possible in this configuration. Degradation such as absorption of atmospheric moisture should be detected easily by the Cr^{3+} ion. It is planned to expand the use of optical probes to the structural investigation of thin sol-gel silica films which have applications for devices such as sensors. The use of energy transfer effects to probe the porosity will be continued. Quantitative relative intensity measurements will be made and decay times as a function of concentration will be measured to exploit the potential of the energy transfer system. Other donor-acceptor pairs e.g. Bi^{3+}-Eu^{3+} are under investigation.

REFERENCES

CHAPTER 1

(1) Alan,P *The Chemistry of Glasses*(1990), second edition, Chapman and Hall.

(2) Cable, M *J Non. Crys. Solids* (1986) **84** 7-16.

(3) Brinker, C.J. *J. Non. Crystalline. Solids* (1988) **100**, 31.

(4) Hench,L.; West,J. *Chem Rev* (1990) **90** 33.

CHAPTER 2

(1) Hench,L.; West,J. *Chem Rev* (1990) **90** 33.

(2) Aelion, A.; Cable, A.; Eirich, F. *J. American Chem Soc* (1950) **72** 5702

(3) Orcel,G. *The Chemistry of Silica* PhD dissertation (1987) University of Florida.

(4) Artaki,F.; Zerda,T.; Jonas, J. *Material Science letters* (1985).

(5) Brinker, C.J.;Scherer,G. *Sol Gel Science* (1990), Academic Press.

(6) Engelhart, V.G.; Altenburg, W.; Hobbel, D.; Waker,W.; Znorg, Z. *J. der Chemie* (1977) **418** 43.

(7) Brinker, C.J.; Scherer, G.W. *J Non. Crys. Solids* (1985) **70** 301.

(8) Brinker, C.J.; Keefer, K.D.; Schaefer, D.W.; *J. Non. Crys. Solids* (1982).

(9) Nogami,M.; Moriya, Y.; *J. Non. Crys. Solids* (1980).

(10) Dewar,M.J.S.; Theul, W.; *J. American Chem. Soc* (1977) **99** 4899.

CHAPTER 3

(1) Imbusch, G.F. *Luminescence Spectroscopy* (1978), Academic press.

(2) Lee, J.D. *A new concise inorganic chemistry* (1977); Van Nostrand Reinhold Co.

(3) Gallagher, P.K. *J. Chem. Phys.* (1964) **4** 10 3061.

(4) Tanabe, Y; Sagano, S *J. Phys. Soc. Japan* (1954) **9** 5 766.

(5) Bates, B *Modern Aspects of the Vitreous State* (1962) **1** Butterworths.

(6) Leiblich-Sofer,N; Reisfeld,R; *Inorganic Chimica* (1978) **30** 259-266.

CHAPTER 4

(1) Demas, J.N. *Excited State Lifetime Measurements* (1983) Academic press.

(2) Lempicki et al *J. Chem. Phys* (1981) **74** 10.

(3) Bevington, P.R. *Data Reduction and Error Analysis for the Physical sciences* (1985) McGraw Hill.

CHAPTER 5

(1) Gallagher,P.K. *J. Chem. Phys* (1964) **41** 10 3061.

(2) Brecher,C; Reisberg,A *Phys Rev B* (1976) **13** 1 81

(3) Brinker,C.J.; Scherer,G.W. *Sol Gel Science* (1990), Academic Press.

(4) Ennis,G. *MSc dissertation* (1992), Dublin City University, Dublin 9.

(5) Devlin,K; OKelly,B; Tang,Z.R.; McDonagh,C; McGilp,J.F. *J Non Crys. Solids* (1991) **135** 8

(6) Bates,B. *Modern Aspects of the Vitreous State Vol 1* (1962), Butterworths.

(7)

(8) Nath,P.; Douglas, R.W. *Physics and Chemistry of Glasses* (Dec 1965) **6** 6 197.

CHAPTER 6

(1) Reisfeld et Al *Inorganic Chemica Acta* (1978) **30** 259-266.

(2) Leung,A.F.; La,T.W. *J. Chem. Phys.* (1982) **76** 8.

(3) Azenta et Al *J.Luminescence* (1991) 48 and 49; pp522-526.

(4) Brinker,C.J.; Scherer,G.W. *Sol Gel Science* (1990), Academic Press.

CHAPTER 7

(1) Blasse,G *Energy Transfer Processes in Condensed Matter* (1984), NATO Series B:Physics **114**.

(2) Sharp,E.J.; Miller,J.E. *J. Applied Physics* (1973) **44** 9 4098.

(3) Aleshkevich,N.I.; Komyak,A.I.; Savitskaya,E.L.; Syt'Ko,V.V. *Zhurnal Priklandoni Spektroskopii* **49** 3 444-448

(4) Hench,L.; West,J. *Chem Rev* (1990) **90** 33

CHAPTER 8

(1) Brinker,C.J.; Scherer,G.W. *Sol Gel Science* (1990), Academic Press.

(2) Boulon,G; Moine,B; Bourcet,J.C. *Phys Rev B* (1990) **22** 3 1163-1169.

Appendix 1: Programme Listings

Data Acquisition Programme "Aver2"

This program was used to run the fluorescence scans of the Eu^{3+} doped sol-gel glasses. It provided the spectrometer motor control and performed the data acquisition .

```
 10 REM ****************************
 20 REM **                        **
 30 REM **     LUMINESCENCE       **
 40 REM **                        **
 50 REM **     SIGNAL AVERAGED    **
 60 REM **                        **
 70 REM ****************************
 75 CLS
 77 MODE0
 80 PRINT:PRINT:PRINT
 90 PRINTTAB(5,5)"**************************************"
100 PRINTTAB(5,6)"*                                    *"
110 PRINTTAB(5,7)"*      DATA ACQUISITION PROGRAM      *"
120 PRINTTAB(5,8)"*                                    *"
125 PRINTTAB(5,9)"*      KEVIN DEVLIN D.C.U.           *
130 PRINTTAB(5,9)"**************************************"
132 PRINTTAB(5,12)"OPTIONS AVAILABLE"
133 PRINTTAB(5,14)"(A) Scanning Emission Spectrometer"
134 PRINTTAB(5,16)"(B) Scanning Excitation Spectrometer"
136 INPUTTAB(5,18)"CHOICE=  ";CHS
140 CLS
150 CLOSE#0
160 MODE0
170 A=&FCF0
180 ?(A+11)=&C0:?(A+2)=&70:?(A+4)=6:?(A+5)=0
190  C=0
200 INPUTTAB(5,5)" NUMBER OF SAMPLES PER POINT";AV
210 PRINTTAB(5,15)" CHECK TO SEE IF SLIT IS CLOSED"
220 K=GET
230 FOR T=1 TO 10
240 ?A=16:?(A+12)=&0C:?(A+12)=&0E
250 a=(?(A+1))*16+(?(A))MOD16
260
270 C=C+a
280 PRINTa
290 NEXT
300 B=C DIV 10
310 PRINTTAB(5,15)"BACKGROUND D.C. SIGNAL ="B
320 K=GET
330 CLS
340
350 PRINTTAB(5,5) "ADJUST FOR MAX SIGNAL"
360 PRINTTAB(5,10)"TYPE R TO CONTINUE"
370 K=GET
380 ?(A+12)=&0C:?(A+12)=&0E
390 IN=?(A+1)*16+?(A)MOD16
400 PRINTTAB(5,15)"MAX SIGNAL ="B-IN
410 IF K<>69 AND K<>82 THEN 370
```

```
420 IF K=69 THEN 380
430 PRINT
440 PRINT
450 CLS
460 *DRIVE0
470 PRINT
480 PRINT"SAMPLE SPECTRUM"
490 PRINT
500 a=OPENIN"START":INPUT#a,Start
510 b=OPENIN"END":INPUT#b,End
520 c=OPENIN"Inc":INPUT#c,Inc
530 CLOSE#0
540 PRINT"Starting  wavelength "Start
550 PRINT
560 PRINT"Finishing wavelength "End
570 PRINT
580 PRINT"Incremental rate      "Inc
590 P=(End-Start)/Inc+1
600 PRINT
610 INPUT"Do you want to change wavelength range      y/n"
620 IF GET$="Y" THEN PROCINITIAL
630 MODE4
640 DIM Y(2505):DIM K(1)
650 PROCwave
660 PROCADC
670 PROCDATA
680 PROCSAVE
690 INPUT TAB(0,8)" Do you want a copy on chart recorder    y/n"
700 IF GET$="Y" THEN PROCDAC
710 PROCDRAW
720 PROCLABLE
730 *DRIVE0
740 END
750 DEF PROCINITIAL
760 PRINT:PRINT:PRINT
770 INPUT"Starting wavelength ",Start
780 PRINT
790 INPUT"Finish wavelength   ",End
800 PRINT
810 INPUT"Incremental rate ",Inc
820 P=(End-Start)/Inc+1
830 ENDPROC
840
850 DEF PROCDATA
860 X=0
870 A1=Start:b=1 :d=&FCC0:?(d+3)=128
880 CLS:M=1
890 FOR D=1 TO P
900 PROCAVERAGE
903 IF CHS="A" THEN GOTO 910
905 IF CHS="B" THEN PROCSTEP2
906 GOTO 920
910 PROCSTEP
920 PRINTTAB(5,5)A1
930 MOVE X,Y(D)/2:DRAW X,Y(D)/2
940 X=X+1200/P
950 A1=A1+Inc
```

```
 960 NEXT
 970 ENDPROC
 980 DEF PROCDRAW
 990 MOVE  0,0:DRAW 0,900
1000 DRAW 1200,900:DRAW 1200,0
1010 DRAW 0,0
1020 VDU5
1030 MOVE 250,1000:PRINT"Intensity vs Wavelength  "
1040 MOVE -10,910:PRINT"I":MOVE 590,910:PRINT"I":MOVE 1190,910:PRINT"I"
1050 ENDPROC
1060 DEF PROCLABLE
1070 MOVE -150,950:PRINTStart
1080 MOVE 900,950:PRINTEnd
1090 VDU4
1100 ENDPROC
1110 DEF PROCDAC
1120 A1=Start
1130 FOR D=1 TO P
1140 V=2048-(Y(D))
1150 d?b=(V)DIV16
1160 d?2=((V)MOD16)*(1+16*b)
1170 PRINTTAB(5,5)A1
1180 A1=A1+Inc
1190 FOR I=1 TO 200 :NEXT
1200 NEXTD
1210 ENDPROC
1220
1230
1240 DEF PROCADC
1250 A=&FCF0
1260 ?(A+11)=&C0
1270 ?(A+2)=&70
1280 ?(A+4)=6
1290 ?(A+5)=0
1300 ENDPROC
1310 DEF PROCSAVE
1320 INPUT TAB(0,6)" Do you want to save y/n"
1330 IF GET$="N"  THEN ENDPROC
1340 INPUT TAB(5,8)"Name of file  " BS
1350 Y=OPENOUT(BS)
1360 PRINT#Y,Start,End,Inc
1370 FOR D=1 TO P
1380 PRINT#Y,Y(D)
1390 NEXT
1400 CLOSE#0
1410 ENDPROC
1420 DEF PROCwave
1430 a=OPENOUT"START":PRINT#a,Start
1440 b=OPENOUT"END":PRINT#b,End
1450 c=OPENOUT"INC":PRINT#c,Inc
1460 CLOSE#0
1470 ENDPROC
1480 DEF PROCAVERAGE
1490 YD1=0:YD=0
1500 FOR Q=1 TO AV
1510 ?A=16
1520 ?(A+12)=&EC
```

```
1530 ?(A+12)=&CE
1540 YD=B-(?(A+1)*16+?(A)MOD16)
1550 YD1=YD1+YD
1560 NEXT
1570 Y(D)=YD1/AV
1580 Y(D)=ABS Y(D)
1590 ENDPROC
1600 DEF PROCSTEP
1610 ?&FE62=&03
1620 FOR L=1 TO Inc*100
1630 ?&FE60=1
1640 ?&FE60=0
1650  NEXT
1660 ENDPROC
1670 DEF PROCSTEP2
1680 ?&FE62=&07
1690 FOR L= 1 TO Inc*6
1700 XR=254:YR=250
1710 ?&FE60=XR
1720 FOR K=1 TO 50 :NEXT K
1730 ?&FE60=YR
1740 FOR K=1 TO 50 :NEXT K
1750 NEXT L
1760 ENDPROC
```

Appendix 2 Programme Listings

Data Acquisition and Control Programme "Lifet"

This programme carried out all the lifetime measurements described in this report, saved t data and then called an analysis programme "Compstw",(See Appendix 3).

```
 10
 20 REM            DATA ACQUISITION PROGRAM
 30
 40 REM            FOR SR400 PHOTON COUNTER.
 50
 60 REM           Kevin Devlin 19/10/89 D.C.U.
 70 MODE7
 90 CLS:*SHADOW
100 PRINT TAB(5)"**************************"
110 PRINT TAB(5)"**DATA ACQUISITION PROGRAM**"
120 PRINT TAB(5)"**FOR SR400 PHOTON COUNTER**"
130 PRINT TAB(5)"**************************":PRINT
140 PRINT "PRESS C TO CONTINUE":X$=GET$ :PRINT
150 IF X$="C" ELSE GOTO 90
160 INPUT"SPECTROMETER WAVELENGTH ";SW$ :PRINT
170 INPUT"SLIT WIDTH (mm)        ";SL$:PRINT
180 INPUT"INPUT DATAFILE NAME TO BE STORED ON DISC";F$:PRINT
190 X=OPENIN(":2."+F$)
200 IF X<>0 THEN PRINT"**DATA FILE ALREADY EXISTS**":CLOSE#0:PRINT ELSE 230
210 PRINT"PRESS C TO CONTINUE OR ANY KEY TO RENAME":X$=GET$
220 IF X$="C" THEN 230 ELSE 90
230 *IEEE
240 cmd%=OPENIN("COMMAND")
250 data%=OPENIN("DATA")
260 ESTR$=CHR$(13)+CHR$(10)
270 PRINT#cmd%,"END OF STRING",ESTR$
280 PRINT#cmd%,"BBC DEVICE NO",0
290 PRINT#cmd%,"CLEAR"
300 PRINT#cmd%,"REMOTE ENABLE"
310 PRINT#cmd%,"UNLISTEN"
320 photon%=OPENIN("23")
330
340 REM *********INPUT OF INITIAL SETUP PARAMETERS********
350
360 PRINT#cmd%,"LISTEN",photon%,"EXECUTE"
370 PRINT#data%,"CM;C10;GD0;NP;DL0;GW0;GY0;CP2"
380 PRINT#cmd%,"UNLISTEN"
390 PRINT#cmd%,"TALK",photon%
400 INPUT#data%,CCM$,CC10$,GGD0$,NNP$,DDL0$,GGW0$,GGY0$,CCP2$
410 PRINT#cmd%,"UNTALK"
420 NNP=VAL(NNP$)
425 DIM V(NNP+30),B(NNP+30),Q(NNP+30)
430
440 REM Display of parameters of significance to measurement of lifetimes.
450
460 CLS
470 PRINT TAB(5)"**DATA ACQUISITION PROGRAM**"
480 PRINT TAB(5)"**FOR SR400 PHOTON COUNTER**":PRINT
```

```
490 PRINT "DATA FILE "TAB(20);FS:PRINT
500 REM PRINT"COUNTING MODE"TAB(20);CCMS.PRINT
510 PRINT"NO OF TRIGGERS"TAB(20);CCP2S:PRINT
520 PRINT "NO OF POINTS"TAB(20);NNPS:PRINT
530 PRINT "A DISC LEVEL"TAB(20);DDL0S:PRINT
540 PRINT "GATE A SCAN STEP"TAB(20);GGY0S:PRINT
550 PRINT "GATE A WIDTH"TAB(20);GGW0S:PRINT
560 PRINT "GATE A DELAY"TAB(20);GGD0S:PRINT
565 PRINT"Press COM on SR400 and then ESCAPE to stop scan":PRINT
570 TIME=0:REPEAT:UNTIL TIME =500
580 PRINT:PRINT "AT POINT NUMBER"  :PRINT
590 PRINT""COUNTER READING"" :PRINT
600 REM*****************************************************************
610
620 REM *********START OF DATA ACQUISITION *********
630
640 REM*****************************************************************
650
660 REM*******************Clear counters,Start scan.******************
670
680 PRINT#cmd%,"LISTEN",photon%,"EXECUTE"
690 PRINT#data%,"CR;CS"
700 PRINT#cmd%,"UNLISTEN"
710
720 REM*******************Poll for data ready.***********************
730 $SS1=0:QQA=0:QQB=0
740 PRINT#cmd%,"LISTEN",photon%,"EXECUTE"
750 PRINT#data%,"SS1"
760 PRINT#cmd%,"UNLISTEN"
770 PRINT#cmd%,"TALK",photon%
780 INPUT#data%,SSS1$
790 PRINT#cmd%,"UNTALK"
800 SSS1=VAL(SSS1$)
810 IF SSS1=0 THEN 740
820
830 REM ************************Read data value.********************
840 FOR I=1 TO NNP
850 PRINT#cmd%,"LISTEN",photon%,"EXECUTE"
860 PRINT#data%,"QA"+STR$(I)
865 PRINT#data%,"QB"+STR$(I)
870 PRINT#cmd%,"UNLISTEN"
880 PRINT#cmd%,"TALK",photon%
890 INPUT#data%,QQAS,QQBS
900 PRINT#cmd%,"UNTALK"
910 PRINTTAB(20,20); I-1
920 QQA=VAL(QQAS):QQB=VAL(QQBS)
930 IF QQA=-1 THEN GOTO 850
940 D=I+9:V(D)=QQA:B(D)=QQB
950 PRINT:PRINT:PRINT  QQA
960 NEXT I
970 PRINT#cmd%,"REMOTE DISABLE"
980 CLOSE#photon%
990 CLOSE#data%
1000 CLOSE#cmd%
1010 CLOSE#0
1015 PROCDIVIDE
1020 PROCSAVE
```

```
1025 CHAIN"COMPSTW"
1030 END
1040
1050 REM**********Save data to disk.**********
1060
1070 DEF PROCSAVE
1080 *DISK
1090 Q(0)=VAL(CCMS)
1100 Q(1)=VAL(CCI0S)
1110 Q(2)=VAL(GGD0S)
1120 Q(3)=VAL(NNPS)
1130 Q(4)=VAL(DDL0S)
1140 Q(5)=VAL(GGW0S)
1150 Q(6)=VAL(GGY0S)
1160 Q(7)=VAL(SWS)
1170 Q(8)=VAL(SLS)
1175 Q(9)=VAL(CCP2S)
1180 PRINT:PRINT:PRINT
1190 X=OPENOUT(":2."+FS)
1200 FOR I= 0 TO (NNP+9)
1210 PRINT#X,Q(I)
1220 NEXTI
1230 CLOSE#0
1240 ENDPROC
1250
1260 REM**********Stop scan.**********
1265
1270 DEF PROCCLEAR
1280 PRINT#cmd%,"LISTEN",photon%"EXECUTE"
1290 PRINT#data%,"CH;NE0;ET"
1300 PRINT#cmd%,"UNLISTEN"
1305 FOR I=1 TO 1000:NEXT
1310 ENDPROC
1320
1330 REM**********Calculate true signal.**********
1340
1350 DEF PROCDIVIDE
1355 BMAX=-100
1360 FOR I=10 TO (NNP+9)
1370 IF B(I)>BMAX THEN BMAX=B(I)
1380 NEXT
1390 FOR I=10 TO (NNP+9)
1400 B(I)=B(I)/BMAX
1410 Q(I)=V(I)/B(I)
1420 NEXT
1430 ENDPROC
```

Appendix 3 Programme Listing

Data Analysis Programme "Compstw"

This programme analysed the decay curves using a weighted least squares semi-log plc

```
 10 REM ***********************************************************
 20 REM ****                                                   ****
 30 REM **** 1. Weighted  Least  square  fit of decay curve ****
 40 REM ****             semi-log  plot.                     ****
 50 REM ****                                                   ****
 55 REM **** 2. Component stripping for two component       ****
 56 REM ****                lifetimes.                       ****
 57 REM ****                                                   ****
 60 REM ***********************************************************
 80 CLEAR
 90 *DRIVE2
100 MODE0
110 DIM V(12)
120 *.
130 PRINT:PRINT:PRINT:
140 INPUT"Name of data file" ,B$
150 L=OPENIN(B$)
160 FOR I=0 TO 9
170 INPUT#L,V(I)
180 NEXT
190 CLS
200 CM=V(0):CI=V(1):GD=V(2):NP=V(3):DL=V(4):GW=V(5):GY=V(6)
210 N=NP :time=GY
220 DIM Y(N),Y1(N),Y2(N)
230 FOR i=1 TO N-1:INPUT#L,Y(i):NEXT :CLOSE#0
240 B=0
250 PROCCALCULATE:PROCDRAW:PROCINTENSITY:PROCRESET:PROCDUMP
260 END
270
280 DEF PROCCALCULATE                          :REM  Calculates max
290 YMAX=0:YMIN=100                          :REM  & min values of
300 FOR i=1 TO N-1                         :REM  decay curve.
310 IF Y(i)>YMAX THEN YMAX=Y(i)
320 IF Y(i)<=YMIN THEN YMIN=Y(i)
330 NEXT i
340 ENDPROC
350
360 DEF PROCDRAW                             :REM Plots decay
370 X=100                                  :REM curve on
380 FOR I=1  TO N-1                          :REM monitor.
390 REM Y(I)=Y(I)-YMIN
400 MOVE X,(Y(I)*900/YMAX):DRAW X,(Y(I)*900/YMAX)
410 X=X+1200/N:NEXT
430 ENDPROC
440
450 DEF PROCINTENSITY
460 VDU4:VDU 29,50;950;:X=50
```

```
470 Y1max=-100:Y1min=100
480 PROCCALC2
490 FOR I=1  TO N-1
500 Y=Y1(I)*-900/Y1min
510 MOVE X+2,Y+2:DRAW X-2,Y-2
520 MOVE X-2,Y+2:DRAW X+2,Y-2
530 X=X+1200/N:NEXT I
540 PROCZOOM
550 STA=S:FIN=F
560 T=STA*time:P=FIN -STA:P=P+1
570 w=0:w1=0:w2=0:w3=0:w4=0
580 REM SLOPE OF SLOW COMPONENT
590 FOR O=STA TO FIN
600 PROCSUM :T=T+time:NEXT O
610 PROCSLOPE:PROCEQ
620 w=0:w1=0:w2=0:w3=0:w4=0
630 PROCCALCULATE2
640 T=0:X=50:FOR O=2 TO N
650 Y1(O)=LN(Y2(O)/Imax)
660 Y=Y1(O)*-900/Y1min:MOVEX,Y:DRAW X,Y
670 P=N:PROCSUM:T=T+time
680 X=X+1200/N:NEXT O:PROCSLOPE
690 w=0:w1=0:w2=0:w3=0:w4=0
700 PROCZOOM
710 STA=S:FIN=F:T=(time)*STA
720 FOR O= STA TO FIN
730 Y1(O)=(Y(O)-Y2(O))
740 IF Y1(O)<=0 THEN GOTO 770
750 Y1(O)=LN(Y1(O)/(YMAX-Imax))
760 PROCSUM
770 T=T+time:NEXT O
780 PROCSLOPE:PROCEQ:ENDPROC
790
800 DEF PROCSUM
805 WEIGHT=(1/(Y1(O)*(-1)))
860 w=w+WEIGHT          :REM  sum w
870 w1=w1+WEIGHT*T*Y1(O) :REM  sum t*y
880 w2=w2+WEIGHT*T       :REM  sum t
890 w3=w3+WEIGHT*Y1(O)   :REM  sum y
895 w4=w4+WEIGHT*T*T     :REM  sum sqr t
900 ENDPROC
910
920 DEF PROCSLOPE
935 Slope=((w*w1)-(w2*w3))/((w*w4)-(w2*w2))
940 Intercept=((w4*w3)-(w2*w1))/((w*w4)-(w2*w2))
950 PRINTTAB(0,20)Slope
960 LIFT=-1/Slope
970 PRINTTAB(0,25)LIFT
980 ENDPROC
990
1000 DEF PROCEQ
1010 T1=0:X=50:FOR p=1 TO N
1020 Y1(p)=T1*Slope+Intercept:Y=Y1(p)*-900/Y1min
1030 MOVE X,Y:DRAW X,Y :X=X+1200/N :Y2(p)=EXP(Y1(p))*YMAX
1040 T1=T1+time:NEXT p
1050 ENDPROC
1060
```

```
1070 DEF PROCZOOM
1080 *FX4,1
1090 C=400:hold=0 :M=0 :UZ=0
1100 MOVE C,50:PLOT 6,C,-900
1110 PRINT TAB(0,0);"
1120 PRINT TAB(0,0);"Slow [";CHR$(200);" "CHR$(201);"] Fast[<>] HOLD(H) EXPAND (E) REMOVE
(R)";
1130 XS=GET$
1140 IF XS=CHR$(136) THEN PROCBAR(-1200/N)
1150 IF XS=CHR$(137) THEN PROCBAR(1200/N)
1160 IF XS="H" THEN PROCHOLD
1170 IF XS=">" ORXS="." THEN PROCBAR(10*1200/N)
1180 IF XS="<" ORXS="," THEN PROCBAR(-10*1200/N)
1190 IF XS="R" THEN PROCREMOVE
1200 IF XS="E" THEN PROCEXPAND
1210 IF M=1 THEN GOTO1230
1220 GOTO 1130
1230 ENDPROC
1240
1250 DEF PROCBAR(I)
1260 MOVE C,50:PLOT 6,C,-900
1270 C=C+I
1280 IF C>1250 THEN C=50
1290 IF C<50 THEN C=1250
1300 MOVE C,50:PLOT 6,C,-900
1310 ENDPROC
1320
1330 DEF PROCHOLD
1340 PRINTTAB(0,0)"
1350 IF hold =1 THEN PRINT TAB(0,0);"Point already held press R to remove  ":XS=GET$:GOTO 1450
1360 UZ=1200/N:POINT=((C-50)/UZ)
1370 F=POINT
1380 VDU5
1390 PLOT 4,C,-900
1400 PLOT0,2,-4
1410 PRINT CHR$(202);
1420 VDU4
1430 hold=1
1440 C=C+UZ:MOVE C,50:PLOT 6,C,-900
1450 ENDPROC
1460
1470 DEF PROCREMOVE
1480 IF hold=0 THEN GOTO 1570
1490 J=C
1500 C=INT(POINT)
1510 hold=0
1520 GCOL4,1:PROCHOLD
1530 MOVE C,50:PLOT 6,C,-900:C=C+UZ:MOVE C,50:PLOT 6,C,-900
1540 hold=0
1550 C=J
1560 GCOL0,1
1570 ENDPROC
1580
1590 DEF PROCEXPAND
1600 PRINTTAB(0,0);"
1610 D=((C-50)/UZ)
1620 S=D
```

```
1025 CHAIN"COMPSTW"
1030 END
1040
1050 REM**********Save data to disk.**********
1060
1070 DEF PROCSAVE
1080 *DISK
1090 Q(0)=VAL(CCMS)
1100 Q(1)=VAL(CCI0S)
1110 Q(2)=VAL(GGD0S)
1120 Q(3)=VAL(NNPS)
1130 Q(4)=VAL(DDL0S)
1140 Q(5)=VAL(GGW0S)
1150 Q(6)=VAL(GGY0S)
1160 Q(7)=VAL(SWS)
1170 Q(8)=VAL(SLS)
1175 Q(9)=VAL(CCP2S)
1180 PRINT:PRINT:PRINT
1190 X=OPENOUT(":2."+FS)
1200 FOR I= 0 TO (NNP+9)
1210 PRINT#X,Q(I)
1220 NEXTI
1230 CLOSE#0
1240 ENDPROC
1250
1260 REM**********Stop scan.**********
1265
1270 DEF PROCCLEAR
1280 PRINT#cmd%,"LISTEN",photon%"EXECUTE"
1290 PRINT#data%,"CH;NE0;ET"
1300 PRINT#cmd%,"UNLISTEN"
1305 FOR I=1 TO 1000:NEXT
1310 ENDPROC
1320
1330 REM**********Calculate true signal.**********
1340
1350 DEF PROCDIVIDE
1355 BMAX=-100
1360 FOR I=10 TO (NNP+9)
1370 IF B(I)>BMAX THEN BMAX=B(I)
1380 NEXT
1390 FOR I=10 TO (NNP+9)
1400 B(I)=B(I)/BMAX
1410 Q(I)=V(I)/B(I)
1420 NEXT
1430 ENDPROC
```